Title: SARS-CoV-2-specific CD4$^+$ and CD8$^+$ T cell responses can originate from cross-reactive CMV-specific T cells

Authors: Cilia R Pothast[1]*, Romy C Dijkland[1], Melissa Thaler[3], Renate S Hagedoorn[1], Michel GD Kester[1], Anne K Wouters[1], Pieter S Hiemstra[2], Martijn J van Hemert[3], Stephanie Gras[4,5], JH Frederik Falkenburg[1], Mirjam HM Heemskerk[1]*

Affiliations:

[1] Department of Hematology; Leiden University Medical Center, Leiden, The Netherlands

[2] Department of Pulmonology; Leiden University Medical Center, Leiden, The Netherlands

[3] Department of Medical Microbiology; Leiden University Medical Center, Leiden, The Netherlands

[4] Department of Biochemistry and Chemistry, La Trobe Institute for Molecular Science, La Trobe University, Melbourne, Victoria, Australia;

[5] Department of Biochemistry and Molecular Biology, Monash University, Clayton, Victoria, Australia

***Correspondence:**
Cilia R. Pothast and Mirjam H.M. Heemskerk

Department of Hematology

Leiden University Medical Center

Albinusdreef 2, 2333 ZA Leiden

The Netherlands

+31-(0)71-625-63207

c.r.pothast@lumc.nl and m.h.m.heemskerk@lumc.nl

The authors have declared that no conflict of interest exists.

Abstract

Detection of SARS-coronavirus-2 (SARS-CoV-2) specific $CD4^+$ and $CD8^+$ T cells in SARS-CoV-2-unexposed donors has been explained by the presence of T cells primed by other coronaviruses. However, based on the relative high frequency and prevalence of cross-reactive T cells, we hypothesized CMV may induce these cross-reactive T cells. Stimulation of pre-pandemic cryo-preserved PBMCs with SARS-CoV-2 peptides revealed that frequencies of SARS-CoV-2-specific T cells were higher in CMV-seropositive donors. Characterization of these T cells demonstrated that membrane-specific $CD4^+$ and spike-specific $CD8^+$ T cells originate from cross-reactive CMV-specific T cells. Spike-specific $CD8^+$ T cells recognize SARS-CoV-2 spike peptide FVSNGTHWF (FVS) and dissimilar CMV pp65 peptide IPSINVHHY (IPS) presented by HLA-B*35:01. These dual IPS/FVS-reactive $CD8^+$ T cells were found in multiple donors and shared a common T cell receptor (TCR), illustrating that IPS/FVS-cross-reactivity is caused by a public TCR. Importantly, these cross-reactive T cells reduced spreading of SARS-CoV-2 in airway epithelial Calu-3 cells yet they were not phenotypically activated during late-stage COVID-19, indicating that cross-reactive T cells may more likely play a role during early stage of infection. In conclusion, CMV-specific T cells cross-react with SARS-CoV-2, despite low sequence homology between the two viruses, and may contribute to the pre-existing immunity against SARS-CoV-2.

43 **Main text**

44 Introduction

45 The effectiveness of the innate and adaptive immune system is an important factor for disease
46 outcome during infection with severe acute respiratory syndrome coronavirus 2 (SARS-CoV-2)
47 (Brodin, 2021). $CD4^+$ and $CD8^+$ T cells are important components of the adaptive immune system
48 as $CD4^+$ T cells promote antibody production by B cells and help cytotoxic $CD8^+$ T cells to mediate
49 cytotoxic lysis of SARS-CoV-2 infected cells (Sette & Crotty, 2021). Whilst immunity is commonly
50 measured solely based on antibody titers, research into coronavirus disease (COVID-19)
51 pathophysiology and vaccination effectiveness has associated an effective T cell response with
52 less severe COVID-19 (Bange et al., 2021; Bertoletti et al., 2021; Liao et al., 2020; Rydyznski
53 Moderbacher et al., 2020; Sekine et al., 2020; Sette & Crotty, 2021; A. T. Tan et al., 2021).
54 Additionally, SARS-CoV-2-specific T cell responses have been shown to be present in most
55 individuals 6 months after infection and remain largely unaffected by emerging variants of concern,
56 illustrating their importance in generating durable immune responses (Gao et al., 2022;
57 GeurtsvanKessel et al., 2022; Keeton et al., 2022; Liu et al., 2022; Tarke et al., 2022).

58 Besides *de novo* SARS-CoV-2-specific T cell responses in infected individuals, SARS-CoV-2-
59 specific T cells have also been identified in unexposed individuals (Grifoni et al., 2020; Le Bert et
60 al., 2020; Mateus et al., 2020; Nelde et al., 2021; Weiskopf et al., 2020). This finding indicates that
61 certain T cells which were initially primed against other pathogens are able to recognize an antigen
62 of SARS-CoV-2. This phenomenon is called heterologous immunity and can often be explained by
63 sequence homology between pathogens. Highly homologous sequences are translated into similar
64 proteins which can be processed and presented as epitopes with high sequence similarity in
65 human leukocyte antigen (HLA). For this reason, most research has focused on cross-reactive T
66 cells that are potentially primed by other human coronaviruses (HCoVs) since they share around
67 30% amino acid sequence homology with SARS-CoV-2 (Bacher et al., 2020; Braun et al., 2020;
68 Johansson et al., 2021; Kundu et al., 2022; Le Bert et al., 2020; Loyal et al., 2021; Mateus et al.,
69 2020). However, it has been postulated that SARS-CoV-2-specific T cells in unexposed individuals
70 could also conceivably be primed by other, non-HCoVs (Le Bert et al., 2020; Peng et al., 2020;

71 Stervbo et al., 2020; C. C. S. Tan et al., 2021). Furthermore, previous studies, although limited,
72 have demonstrated the occurrence of cross-reactivity between two epitopes with relatively low
73 sequence homology (Bijen et al., 2018; Cameron et al., 2013; Clute et al., 2005; Cornberg et al.,
74 2010; Riley et al., 2018; Su & Davis, 2013). This form of heterologous immunity is poorly
75 understood and, therefore, predicting such cross-reactivity remains a challenge (Lee et al., 2020).

76 Pre-pandemic SARS-CoV-2-specific T cells are reportedly present in a relatively high proportion
77 of the population, independent of geographical location, indicating that a highly prevalent pathogen
78 could be a potential source of these cross-reactive T cells (Braun et al., 2020; Grifoni et al., 2020;
79 Le Bert et al., 2020; Mateus et al., 2020; Meckiff et al., 2020; Nelde et al., 2021; Sekine et al.,
80 2020; Weiskopf et al., 2020). Furthermore, these cross-reactive T cells should be present in
81 relatively high frequencies, as they are detectable in antigen-induced stimulation assays without
82 additional amplification steps (Braun et al., 2020; Grifoni et al., 2020; Le Bert et al., 2020; Sekine
83 et al., 2020; Weiskopf et al., 2020). Cytomegalovirus (CMV) is a highly prevalent pathogen and
84 usually induces high T cell frequencies, making CMV a potential source for cross-reactive SARS-
85 CoV-2-specific T cells (Sylwester et al., 2005; Zuhair et al., 2019). This is supported by the finding
86 that SARS-CoV-2 cross-reactive $CD8^+$ T cells have been associated with CMV-seropositive
87 (CMV^+) donors (Alanio et al., 2022; Jo et al., 2021). Moreover, previous CMV infection has been
88 associated with severe COVID-19 thereby suggesting a potential role for these cross-reactive T
89 cells. Studies so far indicated that cross-reactive T cells can play a role in COVID-19 but whether
90 they are protective or pathogenic is unclear (Bacher et al., 2020; Kundu et al., 2022). Taking
91 together, we hypothesized that cross-reactive SARS-CoV-2-specific T cells might originate from a
92 memory response against CMV.

93 In the present study, we aimed to identify SARS-CoV-2-specific cross-reactive $CD4^+$ and $CD8^+$ T
94 cells in SARS-CoV-2-unexposed individuals. We found an increased presence of cross-reactive T
95 cells in CMV^+ donors and upon isolation and clonal expansion of the spike-reactive $CD8^+$ and
96 membrane-reactive $CD4^+$ T cells we confirmed that these T cells were reactive against both SARS-
97 CoV-2 and CMV. Interestingly, isolated $CD8^+$ T cells recognizing a previously described CMV
98 epitope IPSINVHHY in HLA-B*35:01 were cross-reactive with dissimilar SARS-CoV-2 spike

99 peptide FVSNGTHWF in HLA-B*35:01, demonstrating that cross-reactivity does not solely depend
100 on peptide sequence homology. The T cell receptor (TCR) isolated from these $CD8^+$ T cells was
101 found in multiple donors showing that pre-pandemic spike-reactive $CD8^+$ T cells can be caused by
102 a public CMV-specific TCR. Based on the reduced activation status compared to other SARS-
103 CoV-2 specific T cells in severe COVID-19 patients, we hypothesize that these cross-reactive T
104 cells are not important for clearing the virus at this late stage of the disease. However, these cross-
105 reactive $CD8^+$ T cells were shown to reduce spreading of SARS-CoV-2 infection *in vitro*, and in 2
106 out of 2 CMV^+ severe COVID-19 patients these cross-reactive T cells were detected. This indicates
107 that early in infection at the stage that no SARS-CoV-2 specific T cells are present yet, these cross-
108 reactive T cells may play a role in reducing or preventing SARS-CoV-2 infection.

109

110

111 Results

112 **SARS-CoV-2-specific T cell responses in SARS-CoV-2-unexposed PBMCs correlate with**
113 **CMV seropositivity**

114 To investigate whether SARS-CoV-2-specific $CD4^+$ and $CD8^+$ T cell responses in SARS-CoV-2-
115 unexposed donors correlate with previous CMV infection, pre-pandemic cryopreserved PBMCs
116 from CMV seropositive (CMV^+, N=28) and CMV seronegative (CMV^-, N=39) healthy individuals
117 were stimulated overnight using SARS-CoV-2 and CMV 15-mer peptide pools. These pools
118 included spike (S, S1 and S+), membrane (M) and nucleocapsid (N) antigens from SARS-CoV-2
119 and the most immunogenic CMV antigen, pp65. Memory SARS-CoV-2-specific $CD4^+$ T cells were
120 characterized as $CD154^+CD137^+$ and memory SARS-CoV-2-specific $CD8^+$ T cells were identified
121 based on expression of CD137 and IFN-y (**Fig. 1A&B** and **S1A**). As expected, all CMV^+ donors
122 displayed a $CD4^+$ and/or $CD8^+$ T cell response upon stimulation with pp65 (**Fig. 1C&E**). No marked
123 increase of $CD4^+$ T cell responses were observed after SARS-CoV-2 spike and nucleocapsid
124 stimulation in the CMV^+ group compared to CMV^-. However, 7 donors in the CMV^+ group displayed
125 a $CD4^+$ T cell response against the membrane peptide pool which was not observed in the CMV^-
126 group (**Fig. 1C**). Furthermore, $CD4^+$ T cell response against the membrane pool was accompanied
127 by a $CD4^+$ T cell response against pp65 (**Fig. 1D**). In addition, $CD8^+$ T cell responses were detected
128 against spike peptides in two CMV^+ donors which were not detected in CMV^- donors (**Fig. 1E**).
129 Interestingly, donors with a high $CD8^+$ T cell response against SARS-CoV-2 spike peptides
130 additionally displayed strong reactivity against pp65 (**Fig. 1F**). Taken together, these results show
131 that SARS-CoV-2-unexposed CMV^+, but not CMV^-, individuals had detectable $CD4^+$ T cell
132 responses against membrane peptides and $CD8^+$ T cells targeting spike peptides. These SARS-
133 CoV-2 responses were accompanied by T cell responses against pp65 and thus may indicate that
134 SARS-CoV-2 T cell responses in pre-pandemic samples potentially are memory T cells targeting
135 pp65.

136

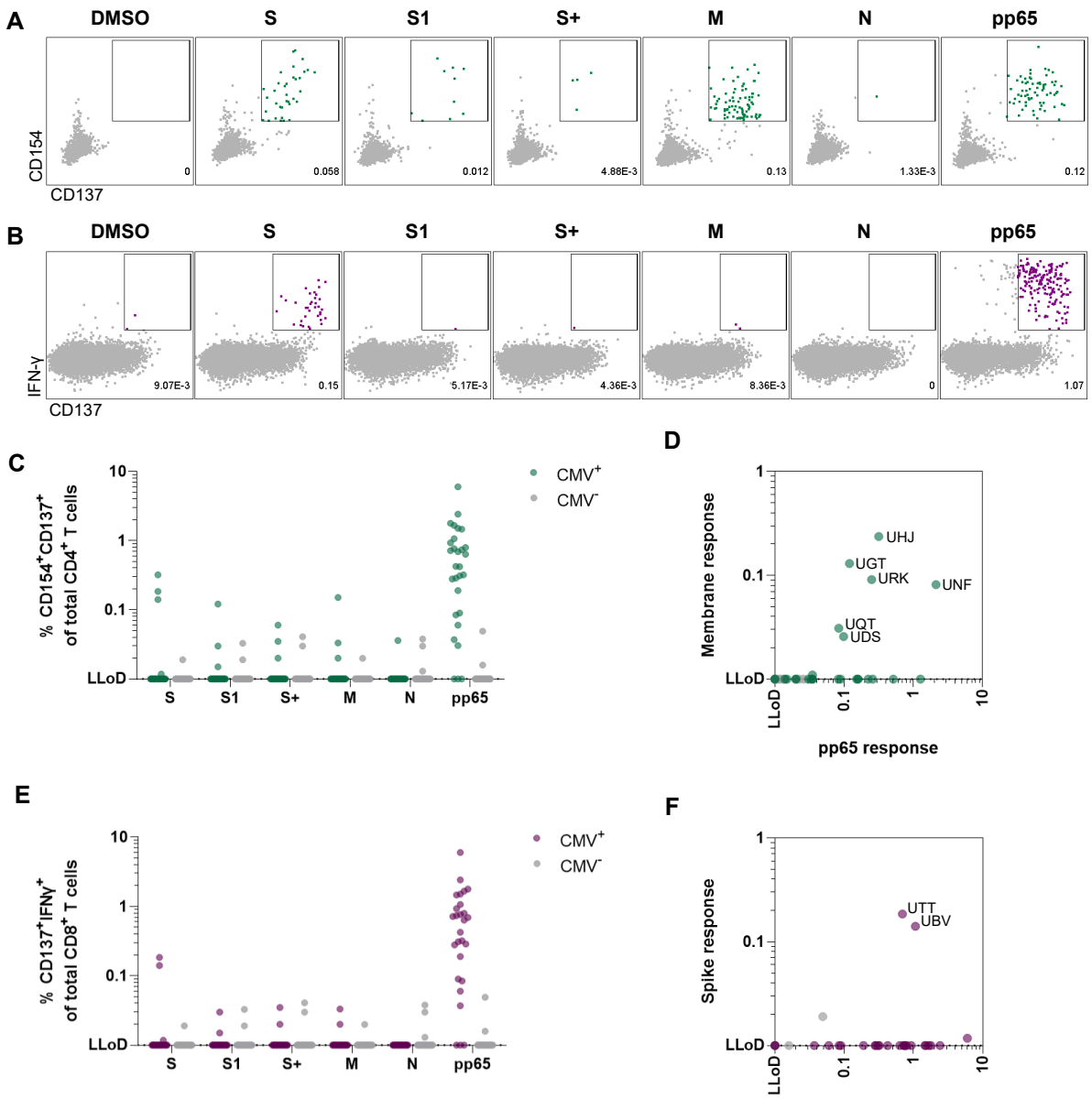

Figure 1 *Ex vivo* SARS-CoV-2-specific CD4⁺ and CD8⁺ T-cell responses in CMV-positive and –negative unexposed donors

Pre-pandemic cryo-preserved PBMCs were stimulated using SARS-CoV-2 spike (S, S1 and S+), membrane (M), nucleocapsid (N) and CMV pp65 peptide pools or not stimulated (DMSO). A) A representative flow cytometry example of a CD4⁺ T cell response in a SARS-CoV-2-unexposed donor. Numbers in plot represent frequencies of CD137⁺CD154⁺ cells of total CD4⁺ T cells. B) A representative flow cytometry example of a CD8⁺ T cell response in a SARS-CoV-2-unexposed donor. Numbers in plot represent frequencies of CD137⁺IFN-γ⁺ cells of total CD8⁺ T cells. C) Scatter plot showing frequencies of CD137⁺CD154⁺ cells of total CD4⁺ T cells of CMV⁺ (green , N=28) and CMV⁻ (grey, N=39) donors. D) Frequencies of CD137⁺CD154⁺ cells of total CD4⁺ T cells

148 in the membrane-stimulated condition (membrane response) plotted against pp65-stimulated
149 condition (pp65 response). 3 letter codes are anonymized codes of CMV^+ (green) and CMV^- (grey)
150 donors. E) Scatter plot showing frequencies of $CD137^+$ IFN-γ^+ cells of total $CD8^+$ T cells of CMV^+
151 (green , N=28) and CMV^- (grey, N=39) donors. F) Frequencies of $CD137^+$IFN-γ^+ cells of total $CD8^+$
152 T cells in the spike-stimulated condition (spike response) plotted against pp65-stimulated condition
153 (pp65 response).

154

155 **Figure 1 – Source data 1**

156 Source data containing the percentages underlying figure 1C-F.

157

158

159 **Pre-pandemic SARS-CoV-2-specific CD4$^+$ and CD8$^+$ T cells recognize pp65 peptides from**
160 **CMV**

161 To confirm that pre-pandemic SARS-CoV-2-specific T cells are able to recognize peptides from
162 pp65, these SARS-CoV-2-specific T cells were isolated and clonally expanded. SARS-CoV-2-
163 unexposed (pre-pandemic cryopreserved) PBMCs from a CMV$^+$ individual showing a CD4$^+$ T cell
164 response against SARS-CoV-2 membrane protein (donor UGT) were stimulated with the
165 membrane peptide pool and single cell sorted based on CD137 upregulation (**Fig. S1B**). After
166 clonal expansion, 20 out of 27 screened T cell clones produced IFN-γ when stimulated with
167 membrane peptide pool compared to no peptide stimulation (data not shown). T cell clones
168 4UGT5, 4UGT8 and 4UGT17, all three expressing a different TCR, were used for further
169 experiments (**Fig. S2A**). As hypothesized, the T cell clones were reactive against both SARS-CoV-
170 2 membrane antigen and CMV pp65 when loaded on HLA-matched Epstein-Barr virus
171 lymphoblastoid cell lines (EBV-LCLs) (**Fig. 2A**). Interestingly, IFN-γ production by the T cell clones
172 was significantly increased when stimulated with pp65 peptides compared to membrane peptides
173 indicating higher avidity for CMV compared to SARS-CoV-2 (**Fig. 2B**). To identify which peptide in
174 pp65 is recognized, reactivity of T cell clone 4UGT8 against a pp65 library was measured which
175 resulted in identification of peptide AGILARNLVPM (**Fig. S2B-C**). HLA-mismatched EBV-LCLs
176 were retrovirally transduced with HLA Class II molecules that were commonly shared between
177 donors that had a detectable CD4$^+$ T cell response against the membrane and pp65 peptide pool
178 (**Fig. 1D**). T cell clone 4UGT8 recognized both peptide pools and the AGI peptide only when
179 presented in HLA-DRB3*02:02 (**Fig. 2C**). The SARS-CoV-2 membrane protein epitope recognized
180 by these cross-reactive T cells remains unidentified. A similar approach was applied for CD8$^+$ T
181 cells in which T cell clones were generated after SARS-CoV-2 spike peptide pool stimulation of
182 PBMCs from CMV$^+$ donor UTT (**Fig. S1B**). The isolated CD8$^+$ T cell clones were screened for their
183 reactivity with SARS-CoV-2 spike which showed that 23 out of the 28 T cell clones produced IFN-
184 γ upon spike peptide pool stimulation (data not shown). TCR sequencing revealed that all 23 T cell
185 clones expressed the same TCR (**Fig. S3A**). T cell clone 8UTT6 was selected for further testing
186 and found to recognize both SARS-CoV-2 spike as well as CMV pp65 peptide pools (**Fig. 2D**). The

187 HLA restriction of T cell clone 8UTT6 was hypothesized to be HLA-B*35:01 as the unexposed
188 donors with a $CD8^+$ T cell response against SARS-CoV-2 spike (UTT and UBV) both expressed
189 HLA-B*35:01. This hypothesis was confirmed as T cell clone 8UTT6 recognized the spike peptide
190 pool presented by K562 cells transduced with HLA-B*35:01 but not transduced with HLA-A*11:01
191 (**Fig. 2E**). To identify the peptide epitopes, reactivity of clone 8UTT6 against 15-mer spike peptide
192 library and nonamer combinatorial peptide library (CPL) was measured followed by netMHC 4.0
193 analysis for predicted binding to HLA-B*35:01, which revealed SARS-CoV-2 peptide
194 FVSNGTHWF (FVS, $S_{1094-1103}$) and CMV IPSINVHHY (IPS, $pp65_{112-121}$) as the most likely epitopes
195 (**Fig. S3B-E**). The FVS and IPS peptides were indeed recognized by clone 8UTT6 (**Fig. 2F**).
196 Importantly, the IPS peptide was recognized with higher avidity compared to the FVS peptide by
197 clone 8UTT6 (**Fig. 2G**). Supporting these findings, the same TCRβ chain was already described
198 and demonstrated to be specific for IPS in HLA-B*35:01 (**Fig. S3E**) (Klarenbeek et al., 2012).
199 Taken together, SARS-CoV-2 reactive $CD4^+$ and $CD8^+$ T cells in pre-pandemic samples cross-
200 reacted with CMV and SARS-CoV-2 peptides.

201

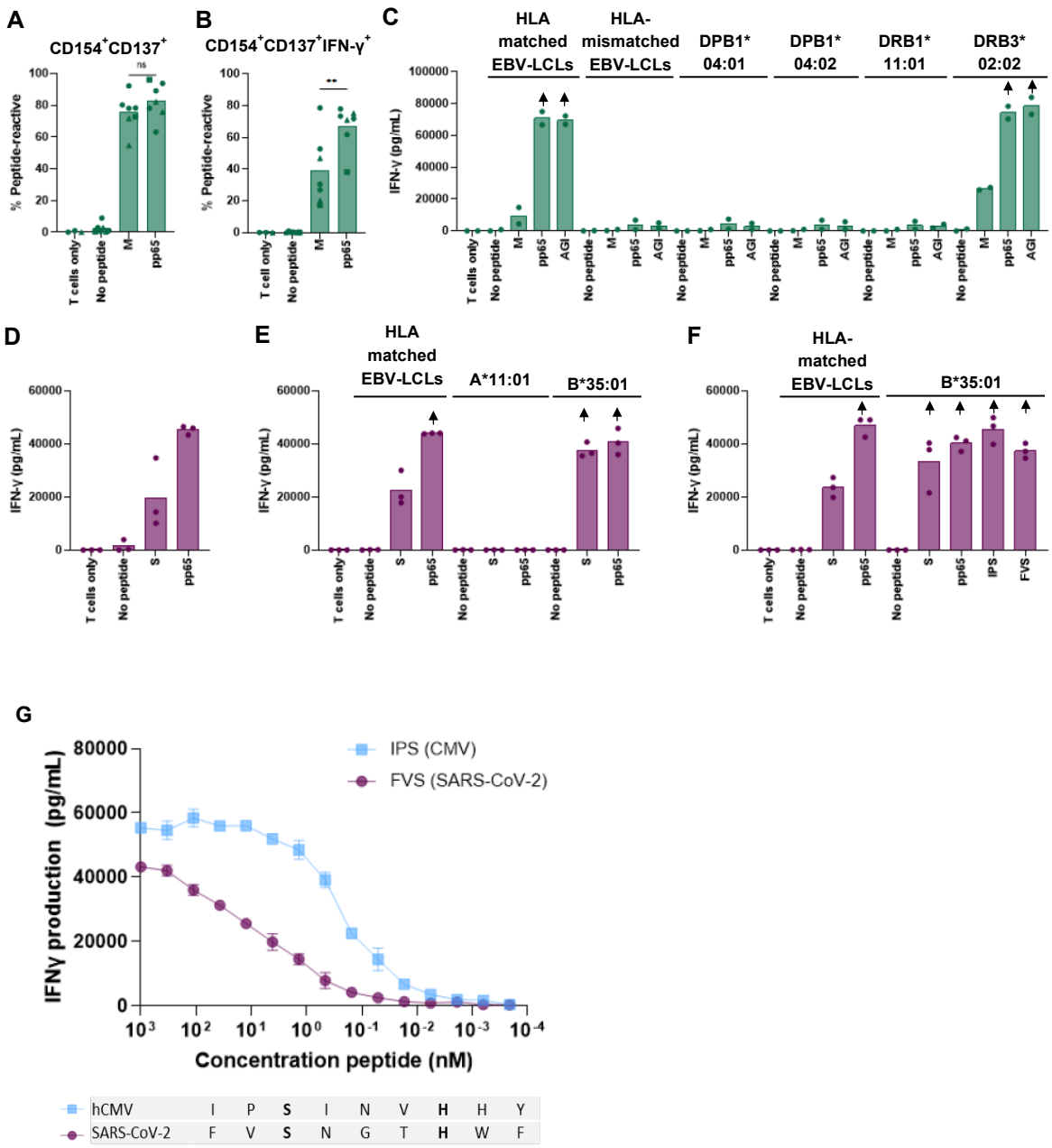
A
CD154+CD137+
% Peptide-reactive
T cells only
No peptide
M
pp65
B
CD154+CD137+IFN-γ+
C
HLA matched EBV-LCLs
HLA-mismatched EBV-LCLs
DPB1* 04:01
DPB1* 04:02
DRB1* 11:01
DRB3* 02:02
IFN-γ (pg/mL)
AGI
D
S
E
A*11:01
B*35:01
F
IPS
FVS
G
IPS (CMV)
FVS (SARS-CoV-2)
IFNγ production (pg/mL)
Concentration peptide (nM)
hCMV I P S I N V H H Y
SARS-CoV-2 F V S N G T H W F

202

203

204

205 **Figure 2** Recognition of SARS-CoV-2 and CMV by pre-existing $CD4^+$ and $CD8^+$ T cells

206 Clonally expanded $CD4^+$ T cells from donor UGT and $CD8^+$ T cells from donor UTT were overnight
207 co-cultured with peptide-pulsed stimulator cells. A-B) Percentages of $CD154^+$, $CD137^+$ and/or IFN-
208 γ^+ cells of T cell clones 4UGT5 (square), 4UGT8 (circles) and 4UGT17 (triangle) after overnight
209 culture (T cells only) or after overnight co-culture with HLA-matched EBV-LCLs that were not
210 peptide pulsed (no peptide) or loaded with membrane (M) or pp65 peptide pool, measured by flow
211 cytometry. Dots represent experimental repeats. Significance was tested by an one-way ANOVA.
212 C) Bar graphs showing ELISA measurement of secreted IFN-γ after co-culturing of a
213 representative clone, 4UGT8 clone, with HLA-matched or HLA-mismatched EBV-LCLs. HLA-
214 mismatched EBV-LCLs were retrovirally transduced with HLA class II molecule as depicted in
215 figure. Targets were peptide-pulsed with membrane (M) peptide pool, pp65 peptide pool or
216 AGILARNLVPM (AGI) peptide. Data points are experimental duplicates. Black arrows indicate that
217 values were above plateau value of the ELISA calibration curve. D-F) Bar graphs showing ELISA
218 measurement of secreted IFN-γ after co-culturing of a representative clone, 8UTT6 clone, with
219 HLA-matched EBV-LCLs or K562s transduced with HLA-B*35:01 or HLA-A*11:01. Targets were
220 peptide-pulsed with spike (S) peptide pool, pp65 peptide pool, IPSINVHHY (IPS) peptide or
221 FVSNGTHWF (FVS) peptide. Data points are technical triplicates. G) Peptide titration of IPS
222 peptide (blue) and FVS peptide (purple) in a co-culture assay with 8UTT6 clone.

223

224

225 **Similarity at the C-terminal part of the peptides could drive T cell cross-reactivity**

226 To understand the molecular basis of T cell cross-reactivity between dissimilar peptides FVS and
227 IPS, we modelled the FVS structure based on the solved structure of the IPS peptide bound to
228 HLA-B*35:01 (**Fig. S4A-B**) (Pellicci et al., 2014). The two peptides share 2 residues (P3-S and P7-
229 H) and also have 2 similar residues (P6-T/V and P9-F/Y). Residue substitutions from the IPS to
230 FVS peptide were possible without major steric clashes with the HLA or peptide residues. The lack
231 of secondary anchor residue at position 5 in the FVS peptide (P5-N/G) might change the
232 conformation of the central part of the peptide, that could be similar to the one observed in the
233 spike-derived peptide IPS ($S_{896-904}$) in complex with HLA-B*35:01 (**Fig. S4C-D**) (Nguyen et al.,
234 2021). The primary anchor in the FVS peptide are P2-V and P9-F, both within the favored residues
235 at those positions for HLA-B35-restricted peptide (Escobar et al., 2008). Overall, the FVS peptide
236 might adopt a similar backbone conformation compared to the IPS peptide, which would place in
237 both peptides a small hydrophobic residue at position 6 (P6-T/V), an histidine at position 7, and a
238 residue with a large side-chain at position 8 (P8-W/H).

239

240 **IPS/FVS-specific cross-reactive CD8$^+$ T cells are detectable in multiple individuals**

241 To investigate the prevalence and phenotype of IPS/FVS cross-reactive T cells, HLA-B*35:01$^+$
242 CMV$^+$ healthy donors were screened for IPS/FVS-specific T cells using tetramers consisting of
243 HLA-B*35:01-FVS (B*35/FVS-tetramer) and HLA-B*35:01-IPS (B*35/IPS-tetramer). Tetramer
244 staining of PBMCs from donor UTT demonstrated that not all T cells that bound to B*35/IPS-
245 tetramer were able to bind to the B*35/FVS-tetramer as well. However, all T cells that bound to
246 B*35/FVS-tetramer were also binding to the B*35/IPS-tetramer (**Fig. 3A**). This observation
247 indicates that IPS/FVS cross-reactivity is dictated by specific TCR sequences which was further
248 supported by the lack of binding to B*35/FVS-tetramer by an IPS-specific T cell clone with a
249 different TCR (**Fig. 3B**). Screening of SARS-CoV-2-unexposed, CMV$^+$ and HLA-B*35(:01) donors
250 (N=37) showed that nearly all CMV$^+$ donors had IPS-specific T cells with frequencies above
251 background level and, interestingly, three of the analyzed donors (UTT, UBV and SFW) presented
252 with clearly detectable IPS/FVS-specific T cells (**Fig. 3C**). Furthermore, IPS/FVS-specific T cells
253 displayed an effector memory phenotype (CCR7$^-$CD45RA$^-$), confirming a memory repertoire origin
254 and, interestingly, a less differentiated phenotype compared to IPS-specific T cells (**Fig. 3D**). In
255 summary, IPS/FVS cross-reactivity is dependent on the TCR clonotype and these cross-reactive
256 T cells are detected in multiple donors.

257

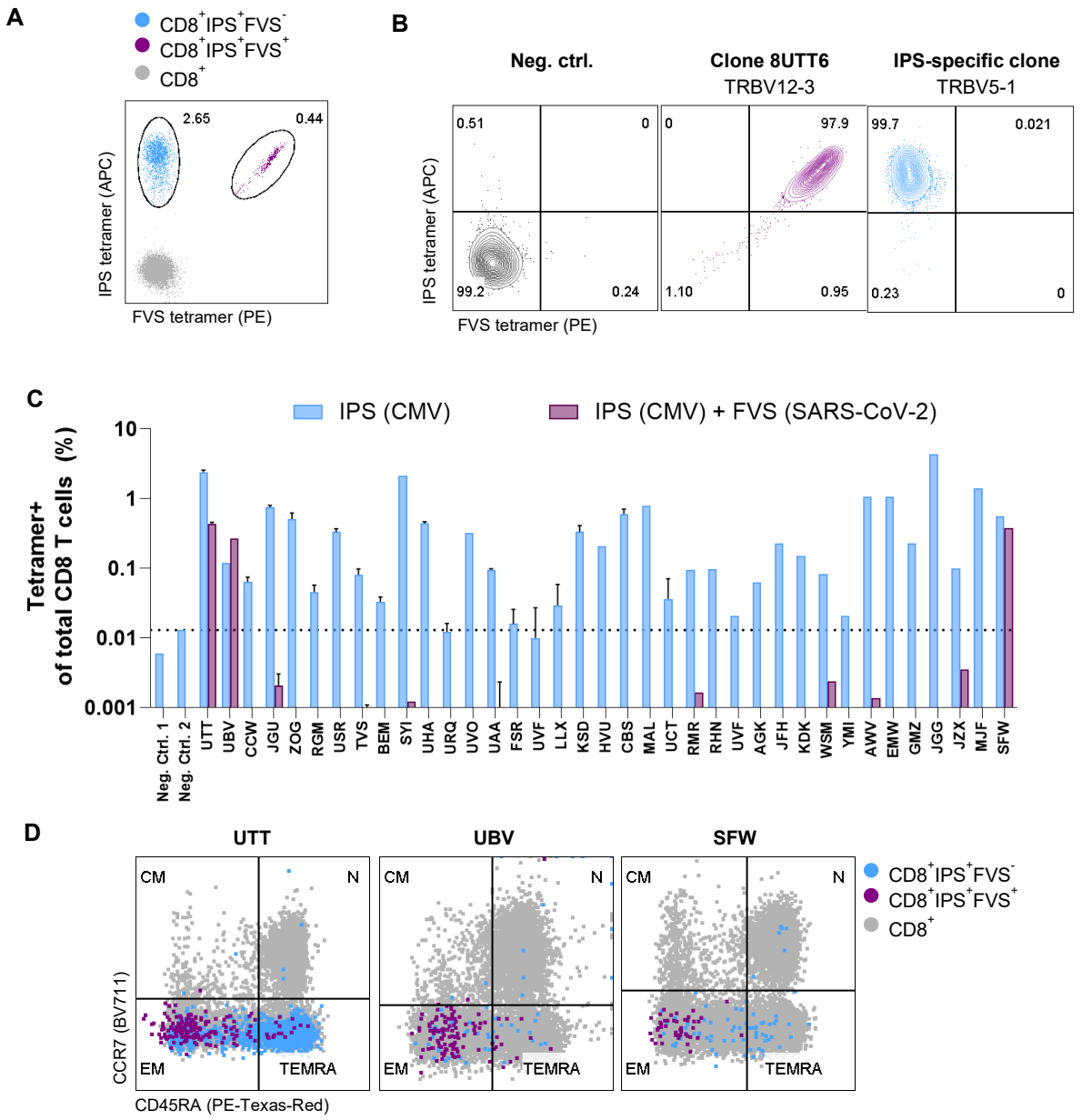

258

259 **Figure 3** Tetramer detection of IPS/FVS-specific CD8⁺ T cells in CMV⁺ and HLA-B*35:01⁺ donors

260 Flow cytometry measurement of PBMCs or T cell clones that are binding to B*35/IPS-tetramer

261 (blue), B*35/FVS-tetramer (purple) or to neither (grey). A) Flow cytometry dot plot showing

262 percentages of tetramer-binding cells of total CD8⁺ T cells in PBMCs from donor UTT. B) Dot plot

263 showing percentages of tetramer-binding of 8UTT6 clone and an IPS-specific clone with their IMGT

264 variable region of T cell receptor β-chain (TRBV) depicted. As a negative control (neg. ctrl.), a T

265 cell clone recognizing a non-relevant peptide in HLA-B*35:01 was included. C) Bar graph showing

266 frequencies of tetramer-binding of total CD8⁺ from PBMCs of healthy CMV⁺ and HLA-B*35(:01)⁺

267 donors. Error bars represent standard deviation of experimental duplicates. Dotted line represents

268 background level which was based on HLA-B*35:01^{-} donors (neg. ctrl). D) Dot plot showing
269 expression of CCR7 and CD45RA by total CD8^{+} T cells and tetramer-binding T cells in PBMCs
270 from UTT, UBV and SFW. Quadrants separates differentiation subsets into naïve (N), central
271 memory (CM), effector memory (EM) and terminally differentiated effector memory (TEMRA).

272

273

274 **IPS/FVS cross-reactivity is underpinned by a public TCR**

275 To investigate whether the IPS/FVS-specific CD8$^+$ T cells found in multiple donors expressed a
276 similar TCR, the TCR α- and β-chains of B*35/FVS-tetramer-binding T cells were sequenced.
277 Sequencing was performed for samples with clear detection of IPS/FVS-specific T cells (UTT,
278 UBV, SFW) and one donor with B*35/FVS-tetramer$^+$ T cells below background level (JZX) (**Fig.**
279 **3C**). Interestingly, B*35/FVS-isolated T cells from all donors displayed amino acid identical
280 dominant complementary-determining region 3 (CDR3) of the α-chain, CAGNQGGKLIF
281 (CDR3α^{CAGNQG}), and β-chain, CASSLALDEQFF (CDR3β^{CASSLA}) (**Fig. 4A**). This observation
282 thereby shows that IPS/FVS cross-reactivity is caused by a public TCR. These identical CDR3s
283 were not a result of sequencing artefact as nucleotide alignment revealed minor differences
284 between samples (**Fig. S5AB**). In addition to B*35/FVS-isolated T cells, T cells that bound
285 B*35/IPS-tetramer were isolated and sequenced in parallel. Both CDR3α^{CAGNQG} and CDR3β^{CASSLA}
286 were identified in all samples and shown to be among the most dominant TCRs. Remarkably, this
287 was also observed in donor JZX which showed IPS/FVS-tetramer$^+$ T cells below background level,
288 indicating that in more than 3 out of 37 donors this public TCR is present. (**Fig. 4C**). Taken together,
289 IPS/FVS-specific T cells express an identical TCR, found in multiple donors, indicating that public
290 TCRs can exhibit cross-reactive properties.

291

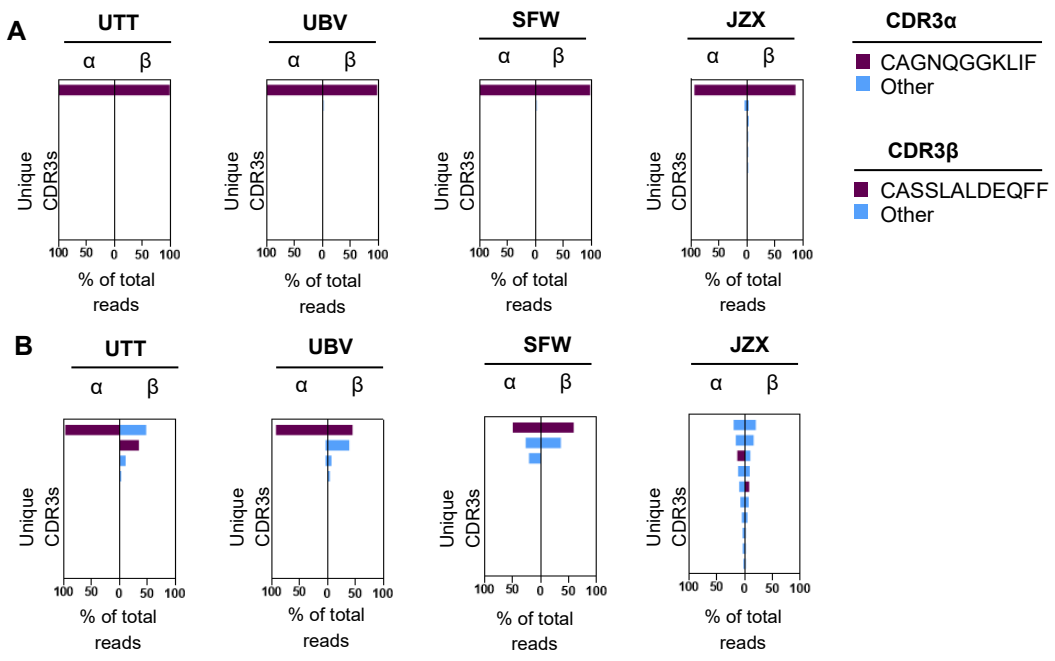

292

293 **Figure 4** TCR sequencing of IPS/FVS-specific T cells

294 PBMCs from healthy CMV⁺ and HLA-B*35:01⁺ donors were sorted on B*35/IPS- or B*35/FVS-
295 tetramer binding and directly sequenced for their TCR alpha and beta chain. Unique CDR3
296 sequences are depicted in two-sided bar graphs in which the left side shows abundance of CDR3
297 sequences from the TCR α-chain (CDR3α) and the right side shows abundance of CDR3
298 sequences from the TCR β-chain (CDR3β). Bar graphs are purple if the CDR3α has the
299 CAGNQGGKLIF sequence or the CDR3β has the CASSLALDEQFF sequence, all other found
300 sequences are depicted in blue. CDR3s with less than 1% abundance were excluded from the
301 figure. A) Two-sided bar graphs showing abundances of unique CDR3 sequences of samples
302 sorted on binding to B*35/FVS-tetramer. B) Two-sided bar graphs showing abundances of unique
303 CDR3 sequences of samples sorted on binding to B*35/IPS-tetramer.

304 **Figure 4 - Source data 1**

305 Source data containing T cell receptor sequence data underlying figure 4.

306

307 **IPS/FVS cross-reactive CD8$^+$ T cells are able to recognize SARS-CoV-2 infected cells but do**
308 **not show an activated phenotype during acute disease**

309 To investigate whether IPS/FVS-specific CD8$^+$ T cells can play a role during SARS-CoV-2
310 infection, the function of IPS/FVS-specific T cells in an *in vitro* model and the activation state of
311 these T cells during acute SARS-CoV-2 infection in severe COVID-19 patients was assessed.
312 Firstly, the reactivity of IPS/FVS-specific T cells against K562 transduced with the spike gene was
313 measured which showed that the T cells were able to recognize endogenously processed and
314 presented peptide (**Fig. 5A**). To investigate whether the IPS/FVS-specific T cells can recognize
315 SARS-CoV-2-infected cells and thereby limit viral spread, Calu-3 airway epithelial cells were
316 infected with live SARS-CoV-2 virus (wildtype) and incubated for 6 hours before co-culturing with
317 CD8$^+$ T cells (**Fig. 5B**). SARS-CoV-2 spike-specific CD8$^+$ T cells from a SARS-CoV-2 vaccinated
318 donor were able to reduce intracellular SARS-CoV-2 RNA copies at both 0.05 and 0.5 MOI 24
319 hours post infection (hpi) (**Fig 5C-D**). Interestingly, IPS/FVS-specific CD8$^+$ T cells were able to
320 reduce SARS-CoV-2 intracellular RNA copies in Calu-3 cells infected with a multiplicity of infection
321 (MOI) (**Fig 5C**). Incubating with 10-fold more virus (0.5 MOI) resulted in no difference in RNA
322 copies compared to the no T cell control (**Fig. 5D**). To further investigate the function of IPS/FVS-
323 specific CD8$^+$ T cells *ex vivo*, the activation state of these T cells was evaluated during severe
324 COVID-19 disease in two CMV$^+$ HLA-B*35:01$^+$ patients. The activation state was measured by
325 expression of activation markers CD38 and HLA-DR as these markers are highly expressed on
326 SARS-CoV-2-specific CD8$^+$ T cells during severe COVID-19 (**Fig. 5E**) (Sekine et al., 2020).
327 Interestingly, IPS/FVS-cross-reactive T cells were detected in 2 out of 2 CMV$^+$ HLA-B*35:01$^+$
328 patients suffering from severe COVID-19, whereas the cross-reactive T cells were detected in 3
329 out of 37 healthy CMV$^+$ HLA-B*35:01$^+$ donors (**Fig. 3C and 5F**). The expression of CD38 and
330 HLA-DR was lower compared to the SARS-CoV-2-specific CD8$^+$ T cells and lower compared to
331 IPS-specific T cells that were not cross-reactive with FVS (**Fig. 5E-F**). These results indicate that
332 IPS/FVS-specific CD8$^+$ T cells recognize SARS-CoV-2-infected cells and are able to limit SARS-
333 CoV-2 replication at low virus titers. However, IPS/FVS-specific T cells did not show an activated
334 phenotype during acute severe SARS-CoV-2 infection.

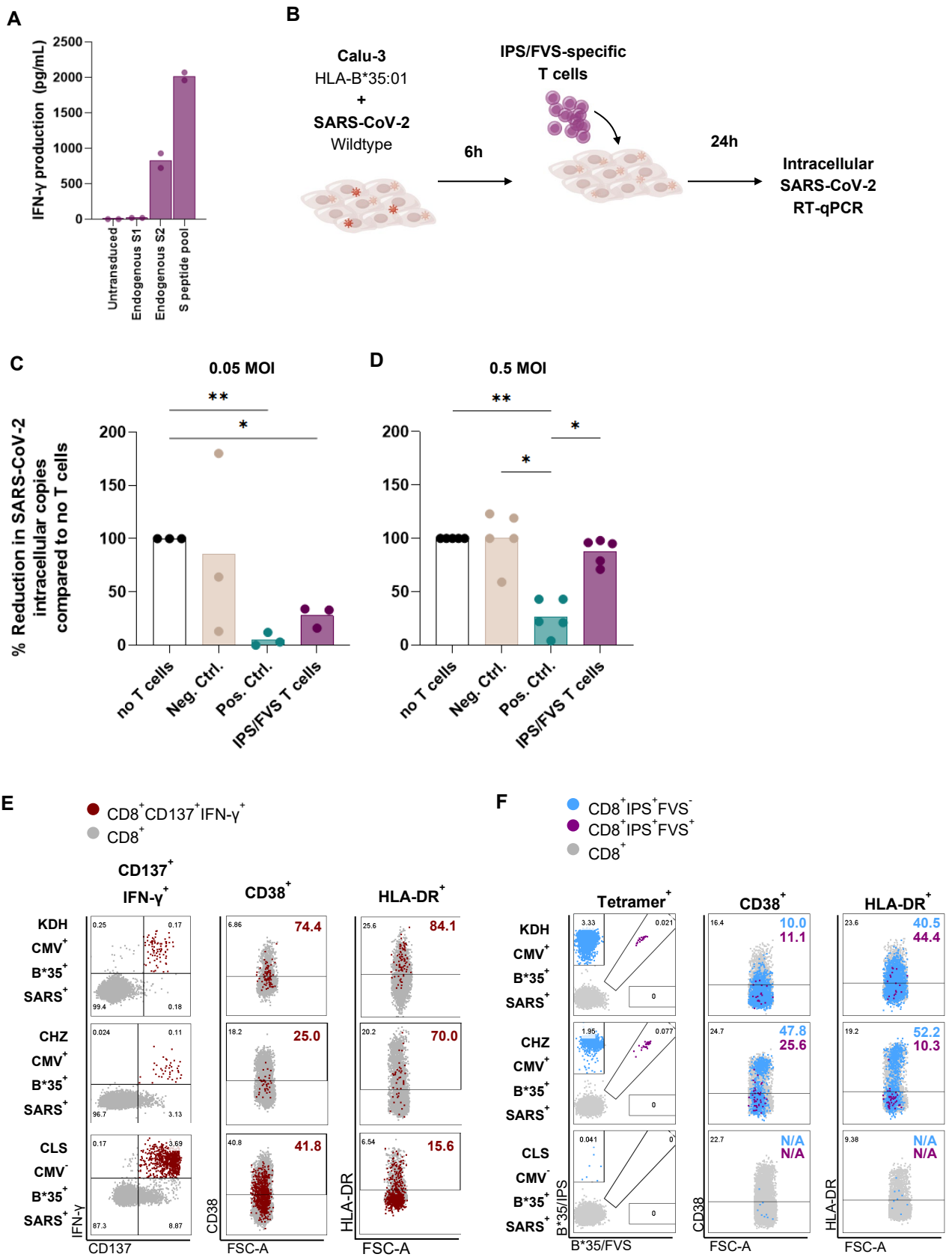
A
IFN-γ production (pg/mL)
2500
2000
1500
1000
500
0
Untransduced
Endogenous S1
Endogenous S2
S peptide pool
B
Calu-3
HLA-B*35:01
+
SARS-CoV-2
Wildtype
6h
IPS/FVS-specific
T cells
24h
Intracellular
SARS-CoV-2
RT-qPCR
C
0.05 MOI
D
0.5 MOI
% Reduction in SARS-CoV-2
intracellular copies
compared to no T cells
no T cells
Neg. Ctrl.
Pos. Ctrl.
IPS/FVS T cells
E
CD8+CD137+IFN-γ+
CD8+
CD137+
IFN-γ+
CD38+
HLA-DR+
KDH
CMV+
B*35+
SARS+
CHZ
CMV+
B*35+
SARS+
CLS
CMV-
B*35+
SARS+
74.4
84.1
25.0
70.0
41.8
15.6
IFN-γ
CD137
CD38
FSC-A
HLA-DR
F
CD8+IPS+FVS-
CD8+IPS+FVS+
CD8+
Tetramer+
CD38+
HLA-DR+
10.0
11.1
40.5
44.4
47.8
25.6
52.2
10.3
N/A
N/A
B*35/IPS
B*35/FVS

335

336 **Figure 5** *Ex vivo* and *in vitro* evaluation of IPS/FVS-specific T cells

337 A) IFN-γ release of IPS/FVS-specific $CD8^+$ T cells after co-incubation with K562 that were
338 untransduced or transduced with nucleotide 1 to 2082 (S1) or nucleotide 2052 to 3822 (S2) of the
339 spike gene. B) Schematic overview of the experimental workflow. Calu-3 cells were transduced to
340 express HLA-B*35:01 and infected with the wildtype SARS-CoV-2 virus. 6 hours post infection,
341 IPS/FVS-specific $CD8^+$ T cells were added in a 10:1 effector to target ratio. SARS-CoV-2 spike-
342 specific T cells, isolated from COVID-19 vaccinated individuals, that recognize VASQSIIAY
343 presented in HLA-B*35:01 (pos. ctrl.) or YLQPRTFLL presented in HLA-A*02:01 (neg. ctrl.) were
344 taken along. Cells were harvested 24 hpi to measure intracellular viral RNA. C-D) Bar graphs
345 showing the means of SARS-CoV-2 intracellular RNA copies measured by RT-qPCR, 24 hpi post
346 infection using a MOI of 0.05 or 0.5. One-way ANOVA was applied test statistical differences
347 between conditions and only comparisons with $p<0.05$ are shown. (E-F) Flow cytometry analysis
348 of CD38 and HLA-DR expression on $CD8^+$ T cells in PBMCs from severe COVID-19 patients that
349 were $CD137^+$IFN-γ^+ after SARS-CoV-2 peptide stimulation (red), only bound to B*35/IPS-tetramer
350 (blue) or bound to both B*35/IPS- and B*35/FVS-tetramer (purple). All other $CD8^+$ T cells are grey.
351 Two patients were HLA-B*35:01$^+$$CMV^+$ (KDH and CHZ) and, as a control, one patient was HLA-
352 B*35:01$^+$$CMV^-$ (CLS). Detection of B*35/IPS- and B*35/FVS-specific T cells and expression of the
353 activation markers were measured and compared within the same sample.

354

355

356 Discussion

357 SARS-CoV-2-specific T cells in pre-pandemic cryo-preserved samples have been reported in
358 several studies. The majority of these studies describe T cell immunity against other HCoVs as the
359 main source of these T cells (Bacher et al., 2020; Braun et al., 2020; Johansson et al., 2021; Kundu
360 et al., 2022; Le Bert et al., 2020; Loyal et al., 2021; Mateus et al., 2020). However, some studies
361 have postulated that pre-pandemic SARS-CoV-2-specific T cells could be derived from other
362 sources (Le Bert et al., 2020; Peng et al., 2020; Stervbo et al., 2020; C. C. S. Tan et al., 2021).
363 Our findings demonstrate that CMV pp65-specific $CD4^+$ T cells cross-react with the membrane
364 protein from SARS-CoV-2 and CMV pp65-specific $CD8^+$ T cells are able to cross-react with SARS-
365 CoV-2 spike protein. The cross-reactive $CD8^+$ T cells recognized known CMV epitope IPSINVHHY
366 in HLA-B*35:01 and cross-reacted with the SARS-CoV-2 epitope FVSNGTHWF in HLA-B*35:01.
367 These IPS/FVS-specific $CD8^+$ T cells were detected in multiple donors all expressing an identical
368 T cell receptor, indicating that cross-reactivity with SARS-CoV-2 can be caused by a CMV-specific
369 public TCR. Functional and phenotypic assessment of the IPS/FVS-specific $CD8^+$ T cells indicated
370 their capacity to reduce SARS-CoV-2 spread *in vitro* but they were not phenotypically active in
371 patients suffering from severe COVID-19.

372 To our knowledge this is the first study to identify CMV-specific T cells that are cross-reactive with
373 SARS-CoV-2. The cross-reactive $CD4^+$ T cells recognized CMV pp65 epitope AGILARNLVPM in
374 HLA-DRB3*02:02 and were able to cross-react with an as of yet unidentified, SARS-CoV-2
375 membrane epitope in HLA-DRB3*02:02. Previous studies have reported the presence of
376 membrane-specific $CD4^+$ T cell responses in SARS-CoV-2-unexposed donors utilizing the same
377 commercially available membrane peptide pool, yet these studies did not aim to identify the
378 peptide-HLA restriction (Bacher et al., 2020; Sekine et al., 2020). The cross-reactive $CD8^+$ T cells
379 recognize the CMV epitope IPSINVHHY and SARS-CoV-2 epitope FVSNGTHWF presented in
380 HLA-B*35:01. IPS/FVS-specific T cells were possibly detected previously but never further
381 investigated or characterized (Shomuradova et al., 2020; Tarke et al., 2021). Both cross-reactive
382 $CD4^+$ and $CD8^+$ T cells displayed a higher avidity for the CMV epitope compared to the epitope
383 derived from SARS-CoV-2. In contrast, other studies have reported an equal or even higher avidity

384 for the SARS-CoV-2 epitope compared to the epitopes derived from the HCoV for which the T cells
385 were hypothesized to be primed against (Braun et al., 2020; Johansson et al., 2021; Lineburg et
386 al., 2021; Mateus et al., 2020). This appears to be contradictive since it has been shown that
387 repeated exposure results in selection of high avidity T cell clonotypes which are able to clear viral
388 infection and protect against reinfection (Abdel-Hakeem et al., 2017; Hombrink et al., 2013; Price
389 et al., 2005; Schober et al., 2018). Cross-reactive T cells would therefore most likely display a
390 higher avidity for the source pathogen compared to the avidity for SARS-CoV-2, as reported in this
391 study. This discrepancy could be caused by the fact that previous studies focused on other HCoVs
392 since they share high sequence homology with SARS-CoV-2, thereby potentially missing the true
393 source of these particular T cells (Bacher et al., 2020; Braun et al., 2020; Johansson et al., 2021;
394 Kundu et al., 2022; Le Bert et al., 2020; Loyal et al., 2021; Mateus et al., 2020). Alternatively,
395 samples frozen down during the pandemic were considered unexposed if the donors displayed
396 neither SARS-CoV-2-specific antibodies nor a history of COVID-19-like symptoms (Bacher et al.,
397 2020; Braun et al., 2020; Lineburg et al., 2021). However, SARS-CoV-2 infection does not
398 necessarily lead to symptoms nor a detectable antibody response (Gao et al., 2021; Steiner et al.,
399 2021). The described reduced avidity for HCoV therefore could imply that these cross-reactive T
400 cells were derived from the SARS-CoV-2-induced repertoire. Taken together, whereas cross-
401 reactive T cells recognizing SARS-CoV-2 have been primarily described to be derived from other
402 HCoVs, the contribution of these other HCoVs as initial primers of the T cell response may have
403 been over-estimated due to experimental design. Further studies are required to identify other
404 potential sources of cross-reactivity with low sequence homology yet high prevalences such as
405 CMV, EBV, influenza or non-viral pathogens.

406 The identified cross-reactive $CD8^+$ T cells appeared to recognize CMV peptide IPSINVHHY and a
407 dissimilar peptide FVSNGTHWF derived from SARS-CoV-2. *Ex vivo* detected heterologous $CD8^+$
408 T cell immunity against two pathogens caused by dissimilar epitopes presented in the same HLA
409 is rarely reported (Clute et al., 2005; Cornberg et al., 2010). Nevertheless, ample studies have
410 investigated the underlying mechanisms of such T cell-mediated cross-reactivity. Heterologous
411 immunity can be caused by the expression of a dual TCR which means that two TCR α- or β-
412 chains are expressed simultaneously, resulting in two distinctive TCRs within one T cell (Cusick et

413 al., 2012). However, here we identified a single TCR in cross-reactive T cells excluding this
414 hypothesis. Recognition of two distinct epitopes by a single TCR can be explained by shape
415 similarity once the peptides are bound to the HLA molecule, and this shape similarity, or molecular
416 mimicry, can underpin T cell cross-reactivity (Macdonald et al., 2009). Possible other underlying
417 mechanisms are reduced footprint of the TCR with peptide (Birnbaum et al., 2014; Cole et al.,
418 2016), an altered TCR-docking angle (Adams et al., 2011), or plasticity of the peptide-MHC
419 complex (Adams et al., 2011; Riley et al., 2018) or TCR (Piepenbrink et al., 2013). Here, similarity
420 between the IPS and FVS peptides in backbone conformation and the C-terminal part might
421 underpin the T cell cross-reactivity observed, as the majority of TCR docks preferentially towards
422 the C-terminal of the peptide (Szeto et al., 2020). Solving the crystal structure of the IPS/FVS-TCR
423 binding to HLA-B*35:01-FVS and -IPS would be necessary to provide insight in the binding
424 properties of the public TCR.

425 IPS/FVS-specific CD8$^+$ T cells were able to reduce SARS-CoV-2 spread *in vitro* when exposed to
426 a low virus concentration, which is supported by our finding that two out of two tested severe
427 COVID-19 patients had clearly detectable IPS/FVS-specific CD8$^+$ T cells while the prevalence in
428 healthy donors was 3 out of 37. The presence of these cross-reactive memory T cells in circulation
429 may be an advantage during initial SARS-CoV-2 infection as rapid T cell responses were
430 associated with less severe COVID-19 (Loyal et al., 2021; Sette & Crotty, 2021; A. T. Tan et al.,
431 2021). However, the cross-reactive CD8$^+$ T cells were less efficient compared to SARS-CoV-2-
432 specific, vaccination-primed T cells in limiting viral spread *in vitro*. This study also demonstrated
433 that IPS/FVS-specific CD8$^+$ T cells did not display the same degree of activation as observed for
434 the SARS-CoV-2-specific T cells during severe COVID-19. Additionally, despite the presence of
435 the cross-reactive CD8$^+$ T cells, these individuals developed severe disease. Their reduced
436 potency is likely caused by intermediate avidity of these cross-reactive T cells for the SARS-CoV-
437 2 epitope which has been associated with poor COVID-19 outcome in case of CD4$^+$ T cells (Bacher
438 et al., 2020). These observations together indicate that IPS/FVS-specific CD8$^+$ T cells might be
439 able to reduce SARS-CoV-2 spread at initial infection, but likely do not play a significant role in the
440 pathogenesis of severe COVID-19. One limitation is that our study focused on circulating T cells,
441 and we cannot exclude the possibility that cross-reactive CD8$^+$ T cells present in lung tissue did

442 display an activated phenotype. Another limitation of this study is the small severe COVID-19
443 cohort that was investigated and literature describing the role of cross-reactive T cells is scarce
444 (Bacher et al., 2020; Kundu et al., 2022). In summary, additional studies using larger cohorts are
445 required to fully elucidate the potential role of cross-reactive $CD8^+$ T cells in disease.

446 In conclusion, pre-pandemic SARS-CoV-2-specific T cells can derive from non-homologous
447 pathogens such as CMV. This expands the potential origin of these pre-pandemic SARS-CoV-2-
448 specific $CD4^+$ and $CD8^+$ T cell beyond other HCoVs. The cross-reactive $CD8^+$ T cells were reactive
449 towards dissimilar epitopes and this cross-reactivity was caused by a public TCR, which has been
450 rarely observed so far. Our data points towards a role of the cross-reactive T cells in reducing
451 SARS-CoV-2 viral load in the early stages of infection, prior to priming of SARS-CoV-2 specific T
452 cells. Altogether, these results aid in further understanding heterologous T cell immunity beyond
453 common cold coronaviruses and facilitates the investigation into the potential role of cross-reactive
454 T cells in COVID-19.

455

456 Methods

457 **Study samples**

458 Bio-banked PBMCs were cryopreserved after informed consent from the respective donors, in
459 accordance with the declaration of Helsinki. The samples from COVID-19 patients were part of a
460 trial (NL8589) registered in the Dutch Trial Registry and approved by Medical Ethical Committee
461 Leiden-Den Haag-Delft (NL73740.058.20). Bio-banked PBMCs from CMV-seropositive (N=28)
462 and CMV-seronegative (N=39) donors that were frozen down before May 2019 were randomly
463 selected to assure that the samples are SARS-CoV-2 naïve and represent the European
464 population (**Table S1**). Prior to cryopreservation, PBMCs were isolated from fresh whole blood
465 using Ficoll-Isopaque. PBMCs were thawed in culture medium consisting of Iscove Modified
466 Dulbecco Medium (IMDM; Lonza, Basel, Switserland) supplemented with 10% heat-inactivated
467 fetal bovine serum (FBS; Sigma-Aldrich, Saint Louis, Missouri), 2.7 mM L-glutamine (Lonza), 100
468 U/mL penicillin (Lonza) and 100 µg/mL streptomycin (Lonza) (1% p/s), and subsequently treated
469 with 1.33 mg/ml DNAse to minimize cell clumping.

470 **Intracellular cytokine staining assay**

471 Thawed PBMCs were stimulated in culture medium supplemented with 1 µg/mL SARS-CoV-2
472 peptides pools covering the spike (Miltenyi, Keulen, Germany), membrane (Miltenyi), or
473 nucleocapsid (Miltenyi) proteins for one hour at 37°C + 5% CO_2. An additional peptide pool
474 containing 11 amino acid overlapping 15-mer peptides covering the pp65 antigen from CMV (JPT
475 Peptide Technologies) was included (see **Table S2** for peptide details). After one hour stimulation,
476 5 µg/mL Brefeldin A (Sigma-Aldrich) was added and the samples were incubated for an additional
477 15 hours at 37°C + 5% CO_2. The samples were subsequently stained with the viability dye Zombie-
478 Red (Biolegend, San Diego, California) for 25 minutes at room temperature (RT) after which the
479 cells were washed in PBS containing 0.8 mg/mL albumin (FACS buffer) and stained with antibodies
480 against CD4 and CD8 in FACS buffer for 30 minutes at 4°C. Cells were washed in PBS and fixed
481 in 1% paraformaldehyde for 8 minutes RT followed by a wash and a permeabilization step for 30
482 minutes at 4°C in FACS buffer supplemented with 1% p/s and 0.1% saponin (permeabilization
483 buffer). After permeabilization, the cells were stained using an antibody cocktail directed against

484 CD14, CD19, CD137, CD154 and IFN-γ in permeabilization buffer (see **Table S3** for antibody
485 details) for 30 minutes at 4°C. After staining, the samples were washed, resuspended in
486 permeabilization buffer and measured on a 3-laser aurora (Cytek Biosciences, Fremont,
487 California).
488

489 **Isolation of SARS-CoV-2-specific T cells**

490 Thawed PBMCs were stimulated for 16 hours at 37°C + 5% CO_2 using 1 µg/mL of spike (Miltenyi)
491 or membrane (Miltenyi) peptide pool in culture medium (see **Table S7** for peptide details). After
492 stimulation, the cells were washed and stained with antibodies directed against CD4, CD8 and
493 CD137 in phenol-red free IMDM (Gibco, Waltham, Massachusetts) containing 2% FBS (Sigma-
494 Aldrich), 1% p/s (Lonza) (sort medium) (see **Table S3** for antibody details) for 30 minutes at 4°C.
495 The cells were subsequently washed and resuspended in sort medium. $CD4^+$ or $CD8^+$ and $CD137^+$
496 cells were single-cell sorted using an Aria III cell sorter (BD Biosciences, Franklin Lakes, New
497 Jersey) into a 96-well round-bottom plate containing $1x10^5$ 35-Gy-irradiated PBMCs, 50-Gy-
498 irradiated EBV-LCL-JYs and 0.8 µg/mL phytohemagglutinin (PHA) (Thermo Fisher, Waltham,
499 Massachusetts) in 100 µL T cell medium (TCM) consisting of IMDM (Lonza) supplemented with
500 2.7 mM L-glutamine (Lonza), 100 U/mL penicillin (Lonza) and 100 µg/mL streptomycin (Lonza),
501 5% FBS (Sigma-Aldrich), 5% human serum (Sanquin, Amsterdam, The Netherlands) and 100
502 IU/mL recombinant human IL-2 (Novartis, Basel, Switzerland). Sorted T cells were clonally
503 expanded to generate T cell clones. T cell clones were restimulated between day 14-20 post
504 stimulation using PHA, PBMCs and EBV-LCL-JYs as described above and used for assays
505 between day 7-20 post stimulation.
506

507 **Co-culture assays**

508 To test peptide and HLA restriction, T cell clones were washed and co-cultured with stimulator
509 cells in a 1:6 effector to stimulator ratio. Stimulator cells consisted of either autologous or HLA-
510 matched EBV-LCLs or retrovirally transduced K562s. K562 were transduced with a pZLRS or
511 MP71 vector containing a HLA gene of interested linked to a marker gene, transduction was

512 performed as previously described (Jahn et al., 2015). Cells were enriched for marker gene
513 expression using magnetic activated cell sorting (MACS; Miltenyi) or fluorescent activated cell
514 sorting (FACS) on an Aria III cell sorter (BD Biosciences). Stimulator cells were loaded with
515 peptides through pre-incubation for 30 minutes at 37°C with 0.01-1 μM peptide (**Table S2** for
516 peptide details). To identify the HLA-restriction of the $CD4^+$ T cell clones, the peptides were not
517 washed away during the co-culture incubation period and HLA class II was knocked out in the T
518 cell clones as previously described (Morton et al., 2020). However, the protocol was adapted to
519 knock-out Class II Major histocompatibility complex transactivator (CIITA) by designing two reverse
520 guide RNAs: 5'-AGTCGCTCACTGGTCCCACTAGG-3' and 5'-
521 CCGTGGACAGTGAATCCACTGGG-3' (Integrated DNA technologies Inc., Coralville, Iowa). Co-
522 culture assays were incubated overnight and secreted IFN-γ was measured as an indicator of T
523 cell activity by ELISA (Diaclone, Besançon, France) as described by the manufacturer.

524 To identify the peptide recognition signature of the CD8 T cell clones, a co-culture assay was
525 performed using a nonamer combinatorial peptide library (CPL) (Bijen et al., 2018). The 9-mer CPL
526 scan contains 180 peptide pools with each pool consisting of a mixture of peptides with one
527 naturally-occurring amino acid fixed at one position (Wooldridge et al., 2010). Co-culture assay
528 was performed as described above with small changes; $2x10^4$ K562 transduced with HLA-B*35:01
529 were pre-incubated with 100 μM CPL peptides for 1 hour at 37°C before $5x10^3$ T cell clones were
530 added. After overnight incubation, secreted IFN-γ was measured by an IFN-γ-ELISA (Diaclone)
531 and results were analyzed using WSBC PI CPL for viruses (Szomolay et al., 2016; Wooldridge,
532 2013). Identified peptides following peptide libraries or CPL were analyzed for predicted binding to
533 HLA-B*35:01 using netMHC 4.0 (Andreatta & Nielsen, 2016). Alternatively, peptide recognition by
534 T cell clones was measured using ICS assay as described above.

535 **Peptide-HLA modelling**

536 The binding of FVS in HLA-B*35:01 was modelled based on the solved crystal structure of the
537 HLA-B*35:01-IPS (Pellicci et al., 2014). Each residue of the IPS peptide was mutated to their
538 corresponding residues in the FVS peptide using the mutagenesis wizard in PyMOL (Schrodinger,

539 2015). The residues were mutated into the most favorable rotamer to avoid steric clashes. No
540 major steric clashes with the peptide or HLA were observed.

541 **TCR variable beta and tetramer staining**

542 PBMCs or T cell clones were incubated with in-house generated, PE- or APC-conjugated tetramers
543 for 30 minutes at RT (Hombrink et al., 2013). After tetramer incubation, the cells were washed and
544 incubated with an antibody mix targeting CD4, CD8, CD45RA, CCR7, CD38 and/or HLA-DR. For
545 TCR variable beta staining, T cell clones were incubated for 30 minutes at 4°C with Beta Mark
546 TCR Vbeta Repertoire Kit (see **Table S3** for antibody details). After incubation, cells were washed
547 and resuspended in FACS buffer and immediately measured on a 3-laser Aurora (Cytek
548 Biosciences).
549

550 **TCR sequencing**

551 PBMCs were thawed and directly stained with PE-conjugated HLA-B*35:01-FVS or HLA-B*35:01-
552 IPS tetramers. Tetramers were labelled to beads using anti-PE MicroBeads (Miltenyi) and enriched
553 through magnetic-activated cell sorting (Miltenyi). The tetramer-enriched cells were washed and
554 incubated with an antibody cocktail targeting CD4 and CD8 (see **Table S3** for antibody details) in
555 sort medium. Stained samples were washed in sort medium and bulk-sorted on an Aria III cell
556 sorter (BD Biosciences) (see **Fig S6B** for a gating example). RNA isolation and TCR sequencing
557 was performed as previously described (Roukens et al., 2022). In short, cells were directly
558 collected in lysis buffer for RNA isolation using the ReliaPrep RNA cell Miniprep system (Promega,
559 Madison, Wisconsin). The total RNA yield of each sample was converted to cDNA using a
560 template-switch oligo primer (TSO) (Eurogentec, Seraing, Belgium), RNAsin (Promega) and
561 SMARTScribe reverse transcriptase (Takara Bio, Kusatsu, Japan) (Koning et al., 2017). cDNA was
562 pre-amplified via an IS region in the Oligo dT primer prior to barcoding on samples containing
563 cDNA from 500 or fewer cells (Picelli et al., 2013). Barcoded TCR PCR product was generated in
564 two rounds of PCR: in the first PCR reaction, *TRA* and *TRB* product was generated in separate
565 PCR reactions using Phusion Flash (Thermo Fisher Scientific), Smartseq2modified PCR primer
566 (Eurogentec) and TRAC or TRBC1/2 specific primers (Eurogentec) (see **Table S4** for primer list).

567 The PCR product was then purified using the Wizard SV 96 PCR Clean-Up System (Promega)
568 and barcoded in a second PCR using two-sided six-nucleotide barcoded primers to discriminate
569 between TCRs of different T cell populations. PCR products of different T cell populations were
570 pooled, after which TCR sequences were identified by NovaSeq (GenomeScan, Leiden, The
571 Netherlands).

572 **SARS-CoV-2 infection assay**

573 Calu-3 lung carcinoma cells (*HTB-55;* ATCC [American Type Culture Collection]) were cultured in
574 Eagle's minimum essential medium (EMEM, Lonza), supplemented with 9% fetal calf serum (FCS;
575 CapriCorn Scientific, USA), 1% NEAA (Sigma-Aldrich), 2 mM L-glutamine (Sigma-Aldrich), 1 mM
576 sodium pyruvate (Sigma-Aldrich) and 100 U/ml of penicillin/streptomycin (P/S; Sigma-Aldrich).
577 Calu-3 cells were retrovirally transduced with a pLZRS vector containing the HLA-B*35:01
578 molecule linked via an internal ribosome entry site (IRES) sequence to mouse CD19, transduction
579 was performed as previously described (Jahn et al., 2015). Mouse CD19 was used as a marker
580 gene to enrich for successfully transduced cells by adding antibodies directed against mouse CD19
581 and enriching for stained cells by MACS (Miltenyi) followed by FACS on an Aria III cell sorter (BD
582 Biosciences) (see **Table S3** for antibody details). For the infection assay, Calu-3 cells were seeded
583 in 96-well cell culture plates at a density of $3x10^4$ cells per well in 100 µl culture medium. Infections
584 were done with clinical isolate SARS-CoV-2/Leiden-0008, which was isolated from a
585 nasopharyngeal sample collected at the LUMC during the first wave of the Corona pandemic in
586 March 2020 (GenBack: MT705206.1). Cells were infected with SARS-CoV-2 at a multiplicity of
587 infection (MOI) of 0.05 or 0.5 in 50 µl infection medium. After 1.5h, cells were washed three times
588 with medium and 100 µl of medium was added. At 6 hours post infection (hpi) medium was
589 removed again and 100 µl of T cell medium with $3x10^5$ T cells per well was added. At 24 hpi cells
590 were harvested to collect intracellular RNA by lysing the cells in 100 µl GITC reagent (3M GITC,
591 2% sarkosyl, 20 mM Tris, 20 mM EDTA) per well. Intracellular RNA was isolated using magnetic
592 beads and viral RNA was quantified by internally controlled multiplex TaqMan RT-qPCR as
593 described previously (Salgado-Benvindo et al., 2020).

594

595 **Statistics**

596 Flow cytometry data was unmixed using Spectroflo (Cytek Biosciences) and analyzed using
597 FlowJo v10.7.1. (BD Biosiences) to set gates on the samples based on the DMSO negative control
598 in ICS assays or adapted to positive control for tetramer staining (see **Fig. S6AB** for a gating
599 example). Samples were excluded from the analysis if less than 10,000 events in $CD4^+$ or $CD8^+$
600 gate was measured or if after further testing they appeared not to be αβ T cells. For the SARS-
601 CoV-2 infection assays, experiments were excluded from the analysis if the positive control had
602 higher SARS-CoV-2 intracellular RNA copies compared to no T cell condition. Statistical analysis
603 and generation of figures was conducted using GraphPad Prism 9.0.1 (GraphPad Software). Data
604 was tested for significance using an one-way ANOVA with *p*-values below 0.05 considered as
605 significant. *p*-values are categorized in the figures as: ns=not significant; *$p<0.05$; **$p<0.01$ or
606 ***$p<0.001$.
607 TCR sequence data were analysed using MiXCR software (v3.0.13) to determine the Vα and Vβ
608 family and CDR3 regions using annotation of the IMGT library (http://www.imgt.org; v6) (Bolotin et
609 al., 2015). CDR3 regions were analysed in RStudio and CDR3 sequences that were non-functional
610 or had ≤50 reads were excluded from the analysis.
611

612 **Author contributions:**

613 Conceptualization: JHFF, MHMH

614 Methodology: CRP, MT, RSH, MGDK, PSH, MJvH, SG, MHMH

615 Investigation: CRP, RCD, MT, RSH, MGDK, AKW

616 Visualization: CRP, SG

617 Funding acquisition: MHMH

618 Project administration: MHMH

619 Supervision: MJvH, JHFF, MHMH

620 Writing – original draft: CRP, SG

621 Writing – review & editing: JHFF, MHMH

622

623

624 **Acknowledgements**

625 The authors like to thank Joost M. Lambooij for critically editing the manuscript. Flow cytometry
626 was performed at the Flow cytometry Core Facility (FCF) of Leiden University Medical Center
627 (LUMC) in Leiden, Netherlands (https://www.lumc.nl/research/facilities/fcf).

628 **Funding:**

629 This study was financially supported by Health~Holland (#LSHM19088) and Australian National
630 Health and Medical Research Council (NHMRC), S.G. is supported by an NHMRC Senior
631 Research Fellowship (#1159272).

632

633

References

Abdel-Hakeem, M. S., Boisvert, M., Bruneau, J., Soudeyns, H., & Shoukry, N. H. (2017). Selective expansion of high functional avidity memory CD8 T cell clonotypes during hepatitis C virus reinfection and clearance. *PLoS Pathog*, *13*(2), e1006191. https://doi.org/10.1371/journal.ppat.1006191

Adams, J. J., Narayanan, S., Liu, B., Birnbaum, M. E., Kruse, A. C., Bowerman, N. A., Chen, W., Levin, A. M., Connolly, J. M., Zhu, C., Kranz, D. M., & Garcia, K. C. (2011). T cell receptor signaling is limited by docking geometry to peptide-major histocompatibility complex. *Immunity*, *35*(5), 681-693. https://doi.org/10.1016/j.immuni.2011.09.013

Alanio, C., Verma, A., Mathew, D., Gouma, S., Liang, G., Dunn, T., Oldridge, D. A., Weaver, J. E., Kuri-Cervantes, L., Pampena, M. B., Unit, U. P. C. P., Betts, M. R., Collman, R. G., Bushman, F. D., Meyer, N. J., Hensley, S. E., Rader, D., & Wherry, E. J. (2022). Cytomegalovirus latent infection is associated with an increased risk of COVID-19-related hospitalization. *J Infect Dis*. https://doi.org/10.1093/infdis/jiac020

Andreatta, M., & Nielsen, M. (2016). Gapped sequence alignment using artificial neural networks: application to the MHC class I system. *Bioinformatics*, *32*(4), 511-517. https://doi.org/10.1093/bioinformatics/btv639

Bacher, P., Rosati, E., Esser, D., Martini, G. R., Saggau, C., Schiminsky, E., Dargvainiene, J., Schroder, I., Wieters, I., Khodamoradi, Y., Eberhardt, F., Vehreschild, M., Neb, H., Sonntagbauer, M., Conrad, C., Tran, F., Rosenstiel, P., Markewitz, R., Wandinger, K. P., Augustin, M., Rybniker, J., Kochanek, M., Leypoldt, F., Cornely, O. A., Koehler, P., Franke, A., & Scheffold, A. (2020). Low-Avidity CD4(+) T Cell Responses to SARS-CoV-2 in Unexposed Individuals and Humans with Severe COVID-19. *Immunity*, *53*(6), 1258-1271 e1255. https://doi.org/10.1016/j.immuni.2020.11.016

Bange, E. M., Han, N. A., Wileyto, P., Kim, J. Y., Gouma, S., Robinson, J., Greenplate, A. R., Hwee, M. A., Porterfield, F., Owoyemi, O., Naik, K., Zheng, C., Galantino, M., Weisman, A. R., Ittner, C. A. G., Kugler, E. M., Baxter, A. E., Oniyide, O., Agyekum, R. S., Dunn, T. G., Jones, T. K., Giannini, H. M., Weirick, M. E., McAllister, C. M., Babady, N. E., Kumar, A., Widman, A. J., DeWolf, S., Boutemine, S. R., Roberts, C., Budzik, K. R., Tollett, S., Wright, C., Perloff, T., Sun, L., Mathew, D., Giles, J. R., Oldridge, D. A., Wu, J. E., Alanio, C., Adamski, S., Garfall, A. L., Vella, L. A., Kerr, S. J., Cohen, J. V., Oyer, R. A., Massa, R., Maillard, I. P., Maxwell, K. N., Reilly, J. P., Maslak, P. G., Vonderheide, R. H., Wolchok, J. D., Hensley, S. E., Wherry, E. J., Meyer, N. J., DeMichele, A. M., Vardhana, S. A., Mamtani, R., & Huang, A. C. (2021). CD8(+) T cells contribute to survival in patients with COVID-19 and hematologic cancer. *Nat Med*, *27*(7), 1280-1289. https://doi.org/10.1038/s41591-021-01386-7

Bertoletti, A., Le Bert, N., Qui, M., & Tan, A. T. (2021). SARS-CoV-2-specific T cells in infection and vaccination. *Cell Mol Immunol*, *18*(10), 2307-2312. https://doi.org/10.1038/s41423-021-00743-3

Bijen, H. M., van der Steen, D. M., Hagedoorn, R. S., Wouters, A. K., Wooldridge, L., Falkenburg, J. H. F., & Heemskerk, M. H. M. (2018). Preclinical Strategies to Identify Off-Target Toxicity of High-Affinity TCRs. *Mol Ther*, *26*(5), 1206-1214. https://doi.org/10.1016/j.ymthe.2018.02.017

Birnbaum, M. E., Mendoza, J. L., Sethi, D. K., Dong, S., Glanville, J., Dobbins, J., Ozkan, E., Davis, M. M., Wucherpfennig, K. W., & Garcia, K. C. (2014). Deconstructing the peptide-MHC specificity of T cell recognition. *Cell*, *157*(5), 1073-1087. https://doi.org/10.1016/j.cell.2014.03.047

Bolotin, D. A., Poslavsky, S., Mitrophanov, I., Shugay, M., Mamedov, I. Z., Putintseva, E. V., & Chudakov, D. M. (2015). MiXCR: software for comprehensive adaptive immunity profiling. *Nat Methods*, *12*(5), 380-381. https://doi.org/10.1038/nmeth.3364

683 Braun, J., Loyal, L., Frentsch, M., Wendisch, D., Georg, P., Kurth, F., Hippenstiel, S., Dingeldey, M.,
684 Kruse, B., Fauchere, F., Baysal, E., Mangold, M., Henze, L., Lauster, R., Mall, M. A., Beyer, K.,
685 Rohmel, J., Voigt, S., Schmitz, J., Miltenyi, S., Demuth, I., Muller, M. A., Hocke, A.,
686 Witzenrath, M., Suttorp, N., Kern, F., Reimer, U., Wenschuh, H., Drosten, C., Corman, V. M.,
687 Giesecke-Thiel, C., Sander, L. E., & Thiel, A. (2020). SARS-CoV-2-reactive T cells in healthy
688 donors and patients with COVID-19. *Nature*, *587*(7833), 270-274.
689 https://doi.org/10.1038/s41586-020-2598-9
690 Brodin, P. (2021). Immune determinants of COVID-19 disease presentation and severity. *Nat Med*,
691 *27*(1), 28-33. https://doi.org/10.1038/s41591-020-01202-8
692 Cameron, B. J., Gerry, A. B., Dukes, J., Harper, J. V., Kannan, V., Bianchi, F. C., Grand, F., Brewer, J. E.,
693 Gupta, M., Plesa, G., Bossi, G., Vuidepot, A., Powlesland, A. S., Legg, A., Adams, K. J., Bennett,
694 A. D., Pumphrey, N. J., Williams, D. D., Binder-Scholl, G., Kulikovskaya, I., Levine, B. L., Riley, J.
695 L., Varela-Rohena, A., Stadtmauer, E. A., Rapoport, A. P., Linette, G. P., June, C. H., Hassan, N.
696 J., Kalos, M., & Jakobsen, B. K. (2013). Identification of a Titin-derived HLA-A1-presented
697 peptide as a cross-reactive target for engineered MAGE A3-directed T cells. *Sci Transl Med*,
698 *5*(197), 197ra103. https://doi.org/10.1126/scitranslmed.3006034
699 Clute, S. C., Watkin, L. B., Cornberg, M., Naumov, Y. N., Sullivan, J. L., Luzuriaga, K., Welsh, R. M., &
700 Selin, L. K. (2005). Cross-reactive influenza virus-specific CD8+ T cells contribute to
701 lymphoproliferation in Epstein-Barr virus-associated infectious mononucleosis. *J Clin Invest*,
702 *115*(12), 3602-3612. https://doi.org/10.1172/JCI25078
703 Cole, D. K., Bulek, A. M., Dolton, G., Schauenberg, A. J., Szomolay, B., Rittase, W., Trimby, A.,
704 Jothikumar, P., Fuller, A., Skowera, A., Rossjohn, J., Zhu, C., Miles, J. J., Peakman, M.,
705 Wooldridge, L., Rizkallah, P. J., & Sewell, A. K. (2016). Hotspot autoimmune T cell receptor
706 binding underlies pathogen and insulin peptide cross-reactivity. *J Clin Invest*, *126*(9), 3626.
707 https://doi.org/10.1172/JCI89919
708 Cornberg, M., Clute, S. C., Watkin, L. B., Saccoccio, F. M., Kim, S. K., Naumov, Y. N., Brehm, M. A.,
709 Aslan, N., Welsh, R. M., & Selin, L. K. (2010). CD8 T cell cross-reactivity networks mediate
710 heterologous immunity in human EBV and murine vaccinia virus infections. *J Immunol*,
711 *184*(6), 2825-2838. https://doi.org/10.4049/jimmunol.0902168
712 Cusick, M. F., Libbey, J. E., & Fujinami, R. S. (2012). Molecular mimicry as a mechanism of
713 autoimmune disease. *Clin Rev Allergy Immunol*, *42*(1), 102-111.
714 https://doi.org/10.1007/s12016-011-8293-8

715 10.1007/s12016-011-8294-7
716 Escobar, H., Crockett, D. K., Reyes-Vargas, E., Baena, A., Rockwood, A. L., Jensen, P. E., & Delgado, J.
717 C. (2008). Large scale mass spectrometric profiling of peptides eluted from HLA molecules
718 reveals N-terminal-extended peptide motifs. *J Immunol*, *181*(7), 4874-4882.
719 https://doi.org/10.4049/jimmunol.181.7.4874
720 Gao, Y., Cai, C., Grifoni, A., Muller, T. R., Niessl, J., Olofsson, A., Humbert, M., Hansson, L., Osterborg,
721 A., Bergman, P., Chen, P., Olsson, A., Sandberg, J. K., Weiskopf, D., Price, D. A., Ljunggren, H.
722 G., Karlsson, A. C., Sette, A., Aleman, S., & Buggert, M. (2022). Ancestral SARS-CoV-2-specific
723 T cells cross-recognize the Omicron variant. *Nat Med*. https://doi.org/10.1038/s41591-022-
724 01700-x
725 Gao, Z., Xu, Y., Sun, C., Wang, X., Guo, Y., Qiu, S., & Ma, K. (2021). A systematic review of
726 asymptomatic infections with COVID-19. *J Microbiol Immunol Infect*, *54*(1), 12-16.
727 https://doi.org/10.1016/j.jmii.2020.05.001
728 GeurtsvanKessel, C. H., Geers, D., Schmitz, K. S., Mykytyn, A. Z., Lamers, M. M., Bogers, S.,
729 Scherbeijn, S., Gommers, L., Sablerolles, R. S. G., Nieuwkoop, N. N., Rijsbergen, L. C., van Dijk,
730 L. L. A., de Wilde, J., Alblas, K., Breugem, T. I., Rijnders, B. J. A., de Jager, H., Weiskopf, D., van
731 der Kuy, P. H. M., Sette, A., Koopmans, M. P. G., Grifoni, A., Haagmans, B. L., & de Vries, R. D.
732 (2022). Divergent SARS CoV-2 Omicron-reactive T- and B cell responses in COVID-19 vaccine
733 recipients. *Sci Immunol*, eabo2202. https://doi.org/10.1126/sciimmunol.abo2202

734 Grifoni, A., Weiskopf, D., Ramirez, S. I., Mateus, J., Dan, J. M., Moderbacher, C. R., Rawlings, S. A.,
735 Sutherland, A., Premkumar, L., Jadi, R. S., Marrama, D., de Silva, A. M., Frazier, A., Carlin, A.
736 F., Greenbaum, J. A., Peters, B., Krammer, F., Smith, D. M., Crotty, S., & Sette, A. (2020).
737 Targets of T Cell Responses to SARS-CoV-2 Coronavirus in Humans with COVID-19 Disease
738 and Unexposed Individuals. *Cell*, *181*(7), 1489-1501 e1415.
739 https://doi.org/10.1016/j.cell.2020.05.015
740 Hombrink, P., Raz, Y., Kester, M. G., de Boer, R., Weissbrich, B., von dem Borne, P. A., Busch, D. H.,
741 Schumacher, T. N., Falkenburg, J. H., & Heemskerk, M. H. (2013). Mixed functional
742 characteristics correlating with TCR-ligand koff -rate of MHC-tetramer reactive T cells within
743 the naive T-cell repertoire. *Eur J Immunol*, *43*(11), 3038-3050.
744 https://doi.org/10.1002/eji.201343397
745 Jahn, L., Hombrink, P., Hassan, C., Kester, M. G., van der Steen, D. M., Hagedoorn, R. S., Falkenburg,
746 J. H., van Veelen, P. A., & Heemskerk, M. H. (2015). Therapeutic targeting of the BCR-
747 associated protein CD79b in a TCR-based approach is hampered by aberrant expression of
748 CD79b. *Blood*, *125*(6), 949-958. https://doi.org/10.1182/blood-2014-07-587840
749 Jo, N., Zhang, R., Ueno, H., Yamamoto, T., Weiskopf, D., Nagao, M., Yamanaka, S., & Hamazaki, Y.
750 (2021). Aging and CMV Infection Affect Pre-existing SARS-CoV-2-Reactive CD8+ T Cells in
751 Unexposed Individuals [Original Research]. *Frontiers in Aging*, *2*.
752 https://doi.org/10.3389/fragi.2021.719342
753 Johansson, A. M., Malhotra, U., Kim, Y. G., Gomez, R., Krist, M. P., Wald, A., Koelle, D. M., & Kwok,
754 W. W. (2021). Cross-reactive and mono-reactive SARS-CoV-2 CD4+ T cells in prepandemic
755 and COVID-19 convalescent individuals. *PLoS Pathog*, *17*(12), e1010203.
756 https://doi.org/10.1371/journal.ppat.1010203
757 Keeton, R., Tincho, M. B., Ngomti, A., Baguma, R., Benede, N., Suzuki, A., Khan, K., Cele, S., Bernstein,
758 M., Karim, F., Madzorera, S. V., Moyo-Gwete, T., Mennen, M., Skelem, S., Adriaanse, M.,
759 Mutithu, D., Aremu, O., Stek, C., du Bruyn, E., Van Der Mescht, M. A., de Beer, Z., de Villiers,
760 T. R., Bodenstein, A., van den Berg, G., Mendes, A., Strydom, A., Venter, M., Giandhari, J.,
761 Naidoo, Y., Pillay, S., Tegally, H., Grifoni, A., Weiskopf, D., Sette, A., Wilkinson, R. J., de
762 Oliveira, T., Bekker, L. G., Gray, G., Ueckermann, V., Rossouw, T., Boswell, M. T., Bihman, J.,
763 Moore, P. L., Sigal, A., Ntusi, N. A. B., Burgers, W. A., & Riou, C. (2022). T cell responses to
764 SARS-CoV-2 spike cross-recognize Omicron. *Nature*. https://doi.org/10.1038/s41586-022-
765 04460-3
766 Klarenbeek, P. L., Remmerswaal, E. B., ten Berge, I. J., Doorenspleet, M. E., van Schaik, B. D., Esveldt,
767 R. E., Koch, S. D., ten Brinke, A., van Kampen, A. H., Bemelman, F. J., Tak, P. P., Baas, F., de
768 Vries, N., & van Lier, R. A. (2012). Deep sequencing of antiviral T-cell responses to HCMV and
769 EBV in humans reveals a stable repertoire that is maintained for many years. *PLoS Pathog*,
770 *8*(9), e1002889. https://doi.org/10.1371/journal.ppat.1002889
771 Koning, M. T., Kielbasa, S. M., Boersma, V., Buermans, H. P. J., van der Zeeuw, S. A. J., van Bergen, C.
772 A. M., Cleven, A. H. G., Kluin, P. M., Griffioen, M., Navarrete, M. A., & Veelken, H. (2017).
773 ARTISAN PCR: rapid identification of full-length immunoglobulin rearrangements without
774 primer binding bias. *Br J Haematol*, *178*(6), 983-986. https://doi.org/10.1111/bjh.14180
775 Kundu, R., Narean, J. S., Wang, L., Fenn, J., Pillay, T., Fernandez, N. D., Conibear, E., Koycheva, A.,
776 Davies, M., Tolosa-Wright, M., Hakki, S., Varro, R., McDermott, E., Hammett, S., Cutajar, J.,
777 Thwaites, R. S., Parker, E., Rosadas, C., McClure, M., Tedder, R., Taylor, G. P., Dunning, J., &
778 Lalvani, A. (2022). Cross-reactive memory T cells associate with protection against SARS-CoV-
779 2 infection in COVID-19 contacts. *Nat Commun*, *13*(1), 80. https://doi.org/10.1038/s41467-
780 021-27674-x
781 Le Bert, N., Tan, A. T., Kunasegaran, K., Tham, C. Y. L., Hafezi, M., Chia, A., Chng, M. H. Y., Lin, M.,
782 Tan, N., Linster, M., Chia, W. N., Chen, M. I., Wang, L. F., Ooi, E. E., Kalimuddin, S., Tambyah,
783 P. A., Low, J. G., Tan, Y. J., & Bertoletti, A. (2020). SARS-CoV-2-specific T cell immunity in

784 cases of COVID-19 and SARS, and uninfected controls. *Nature*, *584*(7821), 457-462.
785 https://doi.org/10.1038/s41586-020-2550-z
786 Lee, C. H., Salio, M., Napolitani, G., Ogg, G., Simmons, A., & Koohy, H. (2020). Predicting Cross-
787 Reactivity and Antigen Specificity of T Cell Receptors. *Front Immunol*, *11*, 565096.
788 https://doi.org/10.3389/fimmu.2020.565096
789 Liao, M., Liu, Y., Yuan, J., Wen, Y., Xu, G., Zhao, J., Cheng, L., Li, J., Wang, X., Wang, F., Liu, L., Amit, I.,
790 Zhang, S., & Zhang, Z. (2020). Single-cell landscape of bronchoalveolar immune cells in
791 patients with COVID-19. *Nat Med*, *26*(6), 842-844. https://doi.org/10.1038/s41591-020-
792 0901-9
793 Lineburg, K. E., Grant, E. J., Swaminathan, S., Chatzileontiadou, D. S. M., Szeto, C., Sloane, H.,
794 Panikkar, A., Raju, J., Crooks, P., Rehan, S., Nguyen, A. T., Lekieffre, L., Neller, M. A., Tong, Z.
795 W. M., Jayasinghe, D., Chew, K. Y., Lobos, C. A., Halim, H., Burrows, J. M., Riboldi-Tunnicliffe,
796 A., Chen, W., D'Orsogna, L., Khanna, R., Short, K. R., Smith, C., & Gras, S. (2021). CD8(+) T
797 cells specific for an immunodominant SARS-CoV-2 nucleocapsid epitope cross-react with
798 selective seasonal coronaviruses. *Immunity*, *54*(5), 1055-1065 e1055.
799 https://doi.org/10.1016/j.immuni.2021.04.006
800 Liu, J., Chandrashekar, A., Sellers, D., Barrett, J., Jacob-Dolan, C., Lifton, M., McMahan, K., Sciacca,
801 M., VanWyk, H., Wu, C., Yu, J., Collier, A. Y., & Barouch, D. H. (2022). Vaccines Elicit Highly
802 Conserved Cellular Immunity to SARS-CoV-2 Omicron. *Nature*.
803 https://doi.org/10.1038/s41586-022-04465-y
804 Loyal, L., Braun, J., Henze, L., Kruse, B., Dingeldey, M., Reimer, U., Kern, F., Schwarz, T., Mangold, M.,
805 Unger, C., Dorfler, F., Kadler, S., Rosowski, J., Gurcan, K., Uyar-Aydin, Z., Frentsch, M., Kurth,
806 F., Schnatbaum, K., Eckey, M., Hippenstiel, S., Hocke, A., Muller, M. A., Sawitzki, B., Miltenyi,
807 S., Paul, F., Mall, M. A., Wenschuh, H., Voigt, S., Drosten, C., Lauster, R., Lachman, N., Sander,
808 L. E., Corman, V. M., Rohmel, J., Meyer-Arndt, L., Thiel, A., & Giesecke-Thiel, C. (2021). Cross-
809 reactive CD4(+) T cells enhance SARS-CoV-2 immune responses upon infection and
810 vaccination. *Science*, *374*(6564), eabh1823. https://doi.org/10.1126/science.abh1823
811 Macdonald, W. A., Chen, Z., Gras, S., Archbold, J. K., Tynan, F. E., Clements, C. S., Bharadwaj, M.,
812 Kjer-Nielsen, L., Saunders, P. M., Wilce, M. C., Crawford, F., Stadinsky, B., Jackson, D., Brooks,
813 A. G., Purcell, A. W., Kappler, J. W., Burrows, S. R., Rossjohn, J., & McCluskey, J. (2009). T cell
814 allorecognition via molecular mimicry. *Immunity*, *31*(6), 897-908.
815 https://doi.org/10.1016/j.immuni.2009.09.025
816 Mateus, J., Grifoni, A., Tarke, A., Sidney, J., Ramirez, S. I., Dan, J. M., Burger, Z. C., Rawlings, S. A.,
817 Smith, D. M., Phillips, E., Mallal, S., Lammers, M., Rubiro, P., Quiambao, L., Sutherland, A.,
818 Yu, E. D., da Silva Antunes, R., Greenbaum, J., Frazier, A., Markmann, A. J., Premkumar, L., de
819 Silva, A., Peters, B., Crotty, S., Sette, A., & Weiskopf, D. (2020). Selective and cross-reactive
820 SARS-CoV-2 T cell epitopes in unexposed humans. *Science*, *370*(6512), 89-94.
821 https://doi.org/10.1126/science.abd3871
822 Meckiff, B. J., Ramirez-Suastegui, C., Fajardo, V., Chee, S. J., Kusnadi, A., Simon, H., Eschweiler, S.,
823 Grifoni, A., Pelosi, E., Weiskopf, D., Sette, A., Ay, F., Seumois, G., Ottensmeier, C. H., &
824 Vijayanand, P. (2020). Imbalance of Regulatory and Cytotoxic SARS-CoV-2-Reactive CD4(+) T
825 Cells in COVID-19. *Cell*, *183*(5), 1340-1353 e1316. https://doi.org/10.1016/j.cell.2020.10.001
826 Morton, L. T., Reijmers, R. M., Wouters, A. K., Kweekel, C., Remst, D. F. G., Pothast, C. R., Falkenburg,
827 J. H. F., & Heemskerk, M. H. M. (2020). Simultaneous Deletion of Endogenous TCRalphabeta
828 for TCR Gene Therapy Creates an Improved and Safe Cellular Therapeutic. *Mol Ther*, *28*(1),
829 64-74. https://doi.org/10.1016/j.ymthe.2019.10.001
830 Nelde, A., Bilich, T., Heitmann, J. S., Maringer, Y., Salih, H. R., Roerden, M., Lubke, M., Bauer, J.,
831 Rieth, J., Wacker, M., Peter, A., Horber, S., Traenkle, B., Kaiser, P. D., Rothbauer, U., Becker,
832 M., Junker, D., Krause, G., Strengert, M., Schneiderhan-Marra, N., Templin, M. F., Joos, T. O.,
833 Kowalewski, D. J., Stos-Zweifel, V., Fehr, M., Rabsteyn, A., Mirakaj, V., Karbach, J., Jager, E.,
834 Graf, M., Gruber, L. C., Rachfalski, D., Preuss, B., Hagelstein, I., Marklin, M., Bakchoul, T.,

835 Gouttefangeas, C., Kohlbacher, O., Klein, R., Stevanovic, S., Rammensee, H. G., & Walz, J. S.
836 (2021). SARS-CoV-2-derived peptides define heterologous and COVID-19-induced T cell
837 recognition. *Nat Immunol*, *22*(1), 74-85. https://doi.org/10.1038/s41590-020-00808-x
838 Nguyen, A. T., Szeto, C., Jayasinghe, D., Lobos, C. A., Halim, H., Chatzileontiadou, D. S. M., Grant, E. J.,
839 & Gras, S. (2021). SARS-CoV-2 Spike-Derived Peptides Presented by HLA Molecules.
840 *Biophysica*, *1*(2), 194-203. https://www.mdpi.com/2673-4125/1/2/15
841 Pellicci, D. G., Uldrich, A. P., Le Nours, J., Ross, F., Chabrol, E., Eckle, S. B., de Boer, R., Lim, R. T.,
842 McPherson, K., Besra, G., Howell, A. R., Moretta, L., McCluskey, J., Heemskerk, M. H., Gras,
843 S., Rossjohn, J., & Godfrey, D. I. (2014). The molecular bases of delta/alphabeta T cell-
844 mediated antigen recognition. *J Exp Med*, *211*(13), 2599-2615.
845 https://doi.org/10.1084/jem.20141764
846 Peng, Y., Mentzer, A. J., Liu, G., Yao, X., Yin, Z., Dong, D., Dejnirattisai, W., Rostron, T., Supasa, P., Liu,
847 C., Lopez-Camacho, C., Slon-Campos, J., Zhao, Y., Stuart, D. I., Paesen, G. C., Grimes, J. M.,
848 Antson, A. A., Bayfield, O. W., Hawkins, D., Ker, D. S., Wang, B., Turtle, L., Subramaniam, K.,
849 Thomson, P., Zhang, P., Dold, C., Ratcliff, J., Simmonds, P., de Silva, T., Sopp, P., Wellington,
850 D., Rajapaksa, U., Chen, Y. L., Salio, M., Napolitani, G., Paes, W., Borrow, P., Kessler, B. M.,
851 Fry, J. W., Schwabe, N. F., Semple, M. G., Baillie, J. K., Moore, S. C., Openshaw, P. J. M.,
852 Ansari, M. A., Dunachie, S., Barnes, E., Frater, J., Kerr, G., Goulder, P., Lockett, T., Levin, R.,
853 Zhang, Y., Jing, R., Ho, L. P., Oxford Immunology Network Covid-19 Response, T. c. C.,
854 Investigators, I. C., Cornall, R. J., Conlon, C. P., Klenerman, P., Screaton, G. R.,
855 Mongkolsapaya, J., McMichael, A., Knight, J. C., Ogg, G., & Dong, T. (2020). Broad and strong
856 memory CD4(+) and CD8(+) T cells induced by SARS-CoV-2 in UK convalescent individuals
857 following COVID-19. *Nat Immunol*, *21*(11), 1336-1345. https://doi.org/10.1038/s41590-020-
858 0782-6
859 Picelli, S., Bjorklund, A. K., Faridani, O. R., Sagasser, S., Winberg, G., & Sandberg, R. (2013). Smart-
860 seq2 for sensitive full-length transcriptome profiling in single cells. *Nat Methods*, *10*(11),
861 1096-1098. https://doi.org/10.1038/nmeth.2639
862 Piepenbrink, K. H., Blevins, S. J., Scott, D. R., & Baker, B. M. (2013). The basis for limited specificity
863 and MHC restriction in a T cell receptor interface. *Nat Commun*, *4*, 1948.
864 https://doi.org/10.1038/ncomms2948
865 Price, D. A., Brenchley, J. M., Ruff, L. E., Betts, M. R., Hill, B. J., Roederer, M., Koup, R. A., Migueles, S.
866 A., Gostick, E., Wooldridge, L., Sewell, A. K., Connors, M., & Douek, D. C. (2005). Avidity for
867 antigen shapes clonal dominance in CD8+ T cell populations specific for persistent DNA
868 viruses. *J Exp Med*, *202*(10), 1349-1361. https://doi.org/10.1084/jem.20051357
869 Riley, T. P., Hellman, L. M., Gee, M. H., Mendoza, J. L., Alonso, J. A., Foley, K. C., Nishimura, M. I.,
870 Vander Kooi, C. W., Garcia, K. C., & Baker, B. M. (2018). T cell receptor cross-reactivity
871 expanded by dramatic peptide-MHC adaptability. *Nat Chem Biol*, *14*(10), 934-942.
872 https://doi.org/10.1038/s41589-018-0130-4
873 Roukens, A. H. E., Pothast, C. R., Konig, M., Huisman, W., Dalebout, T., Tak, T., Azimi, S., Kruize, Y.,
874 Hagedoorn, R. S., Zlei, M., Staal, F. J. T., de Bie, F. J., van Dongen, J. J. M., Arbous, S. M.,
875 Zhang, J. L. H., Verheij, M., Prins, C., van der Does, A. M., Hiemstra, P. S., de Vries, J. J. C.,
876 Janse, J. J., Roestenberg, M., Myeni, S. K., Kikkert, M., Yazdanbakhsh, M., Heemskerk, M. H.
877 M., Smits, H. H., Jochems, S. P., in collaboration with, B.-C. g., & in collaboration with, C.-L. g.
878 (2022). Prolonged activation of nasal immune cell populations and development of tissue-
879 resident SARS-CoV-2-specific CD8(+) T cell responses following COVID-19. *Nat Immunol*,
880 *23*(1), 23-32. https://doi.org/10.1038/s41590-021-01095-w
881 Rydyznski Moderbacher, C., Ramirez, S. I., Dan, J. M., Grifoni, A., Hastie, K. M., Weiskopf, D.,
882 Belanger, S., Abbott, R. K., Kim, C., Choi, J., Kato, Y., Crotty, E. G., Kim, C., Rawlings, S. A.,
883 Mateus, J., Tse, L. P. V., Frazier, A., Baric, R., Peters, B., Greenbaum, J., Ollmann Saphire, E.,
884 Smith, D. M., Sette, A., & Crotty, S. (2020). Antigen-Specific Adaptive Immunity to SARS-CoV-

2 in Acute COVID-19 and Associations with Age and Disease Severity. *Cell*, *183*(4), 996-1012 e1019. https://doi.org/10.1016/j.cell.2020.09.038

Salgado-Benvindo, C., Thaler, M., Tas, A., Ogando, N. S., Bredenbeek, P. J., Ninaber, D. K., Wang, Y., Hiemstra, P. S., Snijder, E. J., & van Hemert, M. J. (2020). Suramin Inhibits SARS-CoV-2 Infection in Cell Culture by Interfering with Early Steps of the Replication Cycle. *Antimicrobial Agents and Chemotherapy*, *64*(8). https://doi.org/ARTN e00900-20

10.1128/AAC.00900-20

Schober, K., Buchholz, V. R., & Busch, D. H. (2018). TCR repertoire evolution during maintenance of CMV-specific T-cell populations. *Immunol Rev*, *283*(1), 113-128. https://doi.org/10.1111/imr.12654

Schrodinger, LLC. (2015). *The PyMOL Molecular Graphics System, Version 1.8*.

Sekine, T., Perez-Potti, A., Rivera-Ballesteros, O., Stralin, K., Gorin, J. B., Olsson, A., Llewellyn-Lacey, S., Kamal, H., Bogdanovic, G., Muschiol, S., Wullimann, D. J., Kammann, T., Emgard, J., Parrot, T., Folkesson, E., Karolinska, C.-S. G., Rooyackers, O., Eriksson, L. I., Henter, J. I., Sonnerborg, A., Allander, T., Albert, J., Nielsen, M., Klingstrom, J., Gredmark-Russ, S., Bjorkstrom, N. K., Sandberg, J. K., Price, D. A., Ljunggren, H. G., Aleman, S., & Buggert, M. (2020). Robust T Cell Immunity in Convalescent Individuals with Asymptomatic or Mild COVID-19. *Cell*, *183*(1), 158-168 e114. https://doi.org/10.1016/j.cell.2020.08.017

Sette, A., & Crotty, S. (2021). Adaptive immunity to SARS-CoV-2 and COVID-19. *Cell*, *184*(4), 861-880. https://doi.org/10.1016/j.cell.2021.01.007

Shomuradova, A. S., Vagida, M. S., Sheetikov, S. A., Zornikova, K. V., Kiryukhin, D., Titov, A., Peshkova, I. O., Khmelevskaya, A., Dianov, D. V., Malasheva, M., Shmelev, A., Serdyuk, Y., Bagaev, D. V., Pivnyuk, A., Shcherbinin, D. S., Maleeva, A. V., Shakirova, N. T., Pilunov, A., Malko, D. B., Khamaganova, E. G., Biderman, B., Ivanov, A., Shugay, M., & Efimov, G. A. (2020). SARS-CoV-2 Epitopes Are Recognized by a Public and Diverse Repertoire of Human T Cell Receptors. *Immunity*, *53*(6), 1245-1257 e1245. https://doi.org/10.1016/j.immuni.2020.11.004

Steiner, S., Schwarz, T., Corman, V. M., Sotzny, F., Bauer, S., Drosten, C., Volk, H. D., Scheibenbogen, C., & Hanitsch, L. G. (2021). Reactive T Cells in Convalescent COVID-19 Patients With Negative SARS-CoV-2 Antibody Serology. *Front Immunol*, *12*, 687449. https://doi.org/10.3389/fimmu.2021.687449

Stervbo, U., Rahmann, S., Roch, T., Westhoff, T. H., & Babel, N. (2020). Epitope similarity cannot explain the pre-formed T cell immunity towards structural SARS-CoV-2 proteins. *Sci Rep*, *10*(1), 18995. https://doi.org/10.1038/s41598-020-75972-z

Su, L. F., & Davis, M. M. (2013). Antiviral memory phenotype T cells in unexposed adults. *Immunol Rev*, *255*(1), 95-109. https://doi.org/10.1111/imr.12095

Sylwester, A. W., Mitchell, B. L., Edgar, J. B., Taormina, C., Pelte, C., Ruchti, F., Sleath, P. R., Grabstein, K. H., Hosken, N. A., Kern, F., Nelson, J. A., & Picker, L. J. (2005). Broadly targeted human cytomegalovirus-specific CD4+ and CD8+ T cells dominate the memory compartments of exposed subjects. *J Exp Med*, *202*(5), 673-685. https://doi.org/10.1084/jem.20050882

Szeto, C., Lobos, C. A., Nguyen, A. T., & Gras, S. (2020). TCR Recognition of Peptide-MHC-I: Rule Makers and Breakers. *Int J Mol Sci*, *22*(1). https://doi.org/10.3390/ijms22010068

Szomolay, B., Liu, J., Brown, P. E., Miles, J. J., Clement, M., Llewellyn-Lacey, S., Dolton, G., Ekeruche-Makinde, J., Lissina, A., Schauenburg, A. J., Sewell, A. K., Burrows, S. R., Roederer, M., Price, D. A., Wooldridge, L., & van den Berg, H. A. (2016). Identification of human viral protein-derived ligands recognized by individual MHCI-restricted T-cell receptors. *Immunol Cell Biol*, *94*(6), 573-582. https://doi.org/10.1038/icb.2016.12

Tan, A. T., Linster, M., Tan, C. W., Le Bert, N., Chia, W. N., Kunasegaran, K., Zhuang, Y., Tham, C. Y. L., Chia, A., Smith, G. J. D., Young, B., Kalimuddin, S., Low, J. G. H., Lye, D., Wang, L. F., & Bertoletti, A. (2021). Early induction of functional SARS-CoV-2-specific T cells associates with

936 rapid viral clearance and mild disease in COVID-19 patients. *Cell Rep*, *34*(6), 108728.
937 https://doi.org/10.1016/j.celrep.2021.108728
938 Tan, C. C. S., Owen, C. J., Tham, C. Y. L., Bertoletti, A., van Dorp, L., & Balloux, F. (2021). Pre-existing T
939 cell-mediated cross-reactivity to SARS-CoV-2 cannot solely be explained by prior exposure to
940 endemic human coronaviruses. *Infect Genet Evol*, *95*, 105075.
941 https://doi.org/10.1016/j.meegid.2021.105075
942 Tarke, A., Coelho, C. H., Zhang, Z., Dan, J. M., Yu, E. D., Methot, N., Bloom, N. I., Goodwin, B., Phillips,
943 E., Mallal, S., Sidney, J., Filaci, G., Weiskopf, D., da Silva Antunes, R., Crotty, S., Grifoni, A., &
944 Sette, A. (2022). SARS-CoV-2 vaccination induces immunological T cell memory able to cross-
945 recognize variants from Alpha to Omicron. *Cell*. https://doi.org/10.1016/j.cell.2022.01.015
946 Tarke, A., Sidney, J., Kidd, C. K., Dan, J. M., Ramirez, S. I., Yu, E. D., Mateus, J., da Silva Antunes, R.,
947 Moore, E., Rubiro, P., Methot, N., Phillips, E., Mallal, S., Frazier, A., Rawlings, S. A.,
948 Greenbaum, J. A., Peters, B., Smith, D. M., Crotty, S., Weiskopf, D., Grifoni, A., & Sette, A.
949 (2021). Comprehensive analysis of T cell immunodominance and immunoprevalence of
950 SARS-CoV-2 epitopes in COVID-19 cases. *Cell Rep Med*, *2*(2), 100204.
951 https://doi.org/10.1016/j.xcrm.2021.100204
952 Weiskopf, D., Schmitz, K. S., Raadsen, M. P., Grifoni, A., Okba, N. M. A., Endeman, H., van den Akker,
953 J. P. C., Molenkamp, R., Koopmans, M. P. G., van Gorp, E. C. M., Haagmans, B. L., de Swart, R.
954 L., Sette, A., & de Vries, R. D. (2020). Phenotype and kinetics of SARS-CoV-2-specific T cells in
955 COVID-19 patients with acute respiratory distress syndrome. *Sci Immunol*, *5*(48).
956 https://doi.org/10.1126/sciimmunol.abd2071
957 Wooldridge, L. (2013). Individual MHCI-Restricted T-Cell Receptors are Characterized by a Unique
958 Peptide Recognition Signature. *Front Immunol*, *4*, 199.
959 https://doi.org/10.3389/fimmu.2013.00199
960 Wooldridge, L., Laugel, B., Ekeruche, J., Clement, M., van den Berg, H. A., Price, D. A., & Sewell, A. K.
961 (2010). CD8 controls T cell cross-reactivity. *J Immunol*, *185*(8), 4625-4632.
962 https://doi.org/10.4049/jimmunol.1001480
963 Zuhair, M., Smit, G. S. A., Wallis, G., Jabbar, F., Smith, C., Devleesschauwer, B., & Griffiths, P. (2019).
964 Estimation of the worldwide seroprevalence of cytomegalovirus: A systematic review and
965 meta-analysis. *Rev Med Virol*, *29*(3), e2034. https://doi.org/10.1002/rmv.2034

966

967 **Supplementary Materials**
968

969 **Figures**

970 Figure S1: Flow cytometry and cell sorting gating example for peptide stimulation assays

971 Figure S2: TCR sequence and pp65 peptide identification of 4UGT8 clone

972 Figure S3: Peptide identification of 8UTT6 clone

973 Figure S4: Model of the HLA-B*35:01-FVS structure

974 Figure S5: TCR sequencing of B*35/FVS-sorted samples

975 Figure S6: Flow cytometry and cell sorting gating example for tetramer staining assays

976

977 **Tables**

978 Table S1: Cohort characteristics

979 Table S2: List of peptides

980 Table S3: List of antibodies and reagents used for flow cytometry

981 Table S4: List of primer sequences used for TCR sequencing

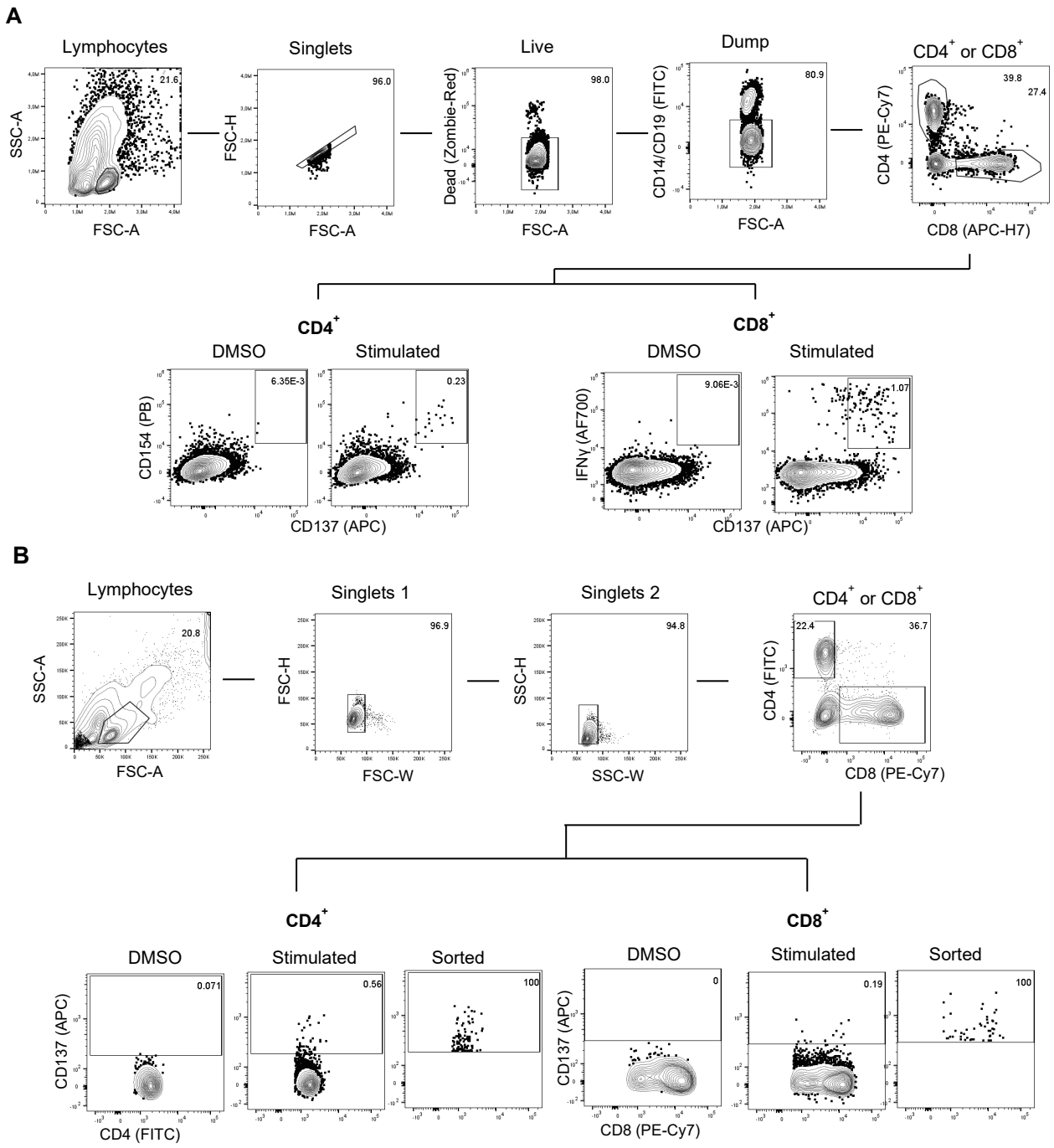
A
Lymphocytes
Singlets
Live
Dump
CD4+ or CD8+
SSC-A
FSC-A
FSC-H
Dead (Zombie-Red)
CD14/CD19 (FITC)
CD4 (PE-Cy7)
CD8 (APC-H7)
21.6
96.0
98.0
80.9
39.8
27.4
CD4+
CD8+
DMSO
Stimulated
CD154 (PB)
CD137 (APC)
IFNγ (AF700)
6.35E-3
0.23
9.06E-3
1.07
B
Lymphocytes
Singlets 1
Singlets 2
CD4+ or CD8+
SSC-A
FSC-A
FSC-H
FSC-W
SSC-H
SSC-W
CD4 (FITC)
CD8 (PE-Cy7)
20.8
96.9
94.8
22.4
36.7
CD4+
CD8+
DMSO
Stimulated
Sorted
CD137 (APC)
CD4 (FITC)
CD8 (PE-Cy7)
0.071
0.56
100
0
0.19
100

982

983 **Supplementary figure 1** Flow cytometry and cell sorting gating example for peptide stimulation
984 assays

985 A) Representative example of flow cytometry gating strategy for peptide-reactive $CD4^+$ and $CD8^+$
986 T cells. All events were gated on lymphocytes, single cells, viable cells, CD14 and CD19 negative
987 and either CD4 or CD8 positive. For $CD4^+$ T cells, activation was measured by upregulation of
988 CD137 and CD154 compared to DMSO. For $CD8^+$ T cells, activation was measured by
989 upregulation of CD137 and IFN-γ production compared to DMSO. B) Representative example of
990 fluorescent-activated cell sorting for peptide-reactive $CD4^+$ and $CD8^+$ T cells. All events were gated
991 on lymphocytes, single cells and subsequently selected for CD4 positive or CD8 positive cells.
992 Activated $CD4^+$ or $CD8^+$ T cells were sorted based on increased expression of CD137 compared
993 to DMSO.

A

Clone #	Chain	CDR3 (aa)	V (IMGT)	J (IMGT)
4UGT5	α	CAMRGVNTGFQKLVF	TRAV14/DV4	TRAJ8
	β	CASSNSGTRIYEQYF	TRBV19	TRBJ2-7
4UGT8	α	CAVDPILTGGGNKLTF	TRAV8-3	TRAJ10
	β	CASSLKRETYNEQFF	TRBV27	TRBV2-1
4UGT17	α	CARGDAGNMLTF	TRAV8-3	TRAJ39
	β	CASSATLGAGNYEQYF	TRBV2	TRBJ2-7

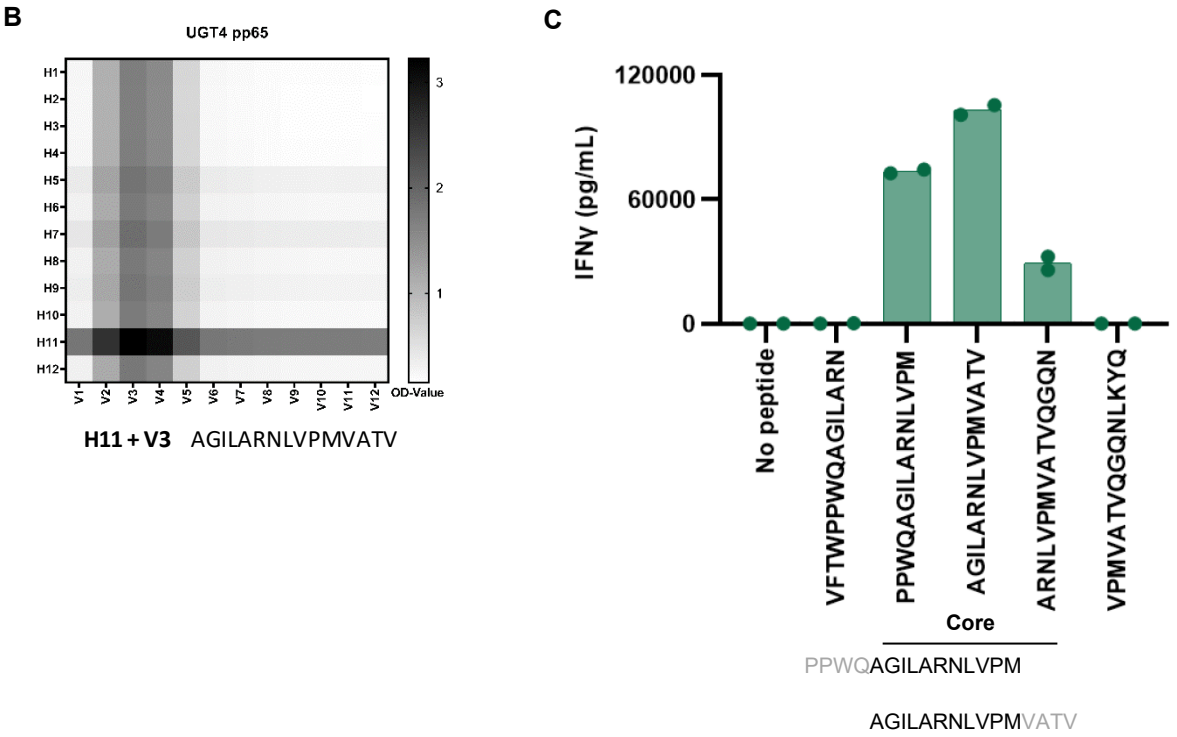

Supplementary figure 2 TCR sequence and pp65 peptide identification of 4UGT8 clone

Reactivity, as measured by IFN-γ ELISA, of the 4UGT8 clone after co-culturing with HLA-matched EBV-LCLs and peptides. A) Heatmap showing reactivity of 4UGT8 clone against a CMV pp65 peptide library, depicted as OD-value. Peptide with highest OD-value is shown below the figure. B) Bar graphs showing IFN-γ secretion after co-culturing 4UGT8 clone with single peptides. Peptides that were recognized were depicted under the figure with amino acid overlap between the peptides in black. Data points are technical duplicates.

A

Chain	CDR3 (aa)	V (IMGT)	J (IMGT)
α	CAGNQGGKLIF	TRAV21*02	TRAJ23*01/2
β	CASSLALDEQFF	TRBV12-3/4*01	TRBJ2-1*01

B

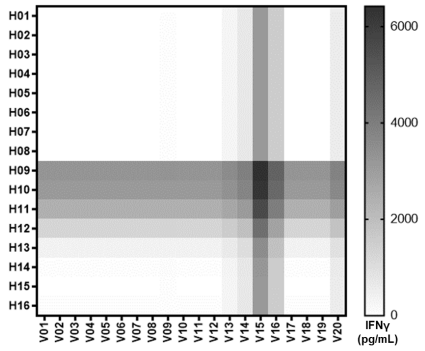

H09+V15 FPREGVFVSNGTHWF

H10+V15 GVFVSNGTHWFVTQR

C

Peptide	Affinity(nM)	Bindlevel
FVSNGTHWF	17.28	<= SB
VFVSNGTHWF	3416.18	
GVFVSNGTH	14798.68	
GVFVSNGTHWF	15539.73	
VSNGTHWF	23385.28	
VFVSNGTHW	26065.08	
FVSNGTHW	27437.91	
GVFVSNGTHW	35804.39	
VFVSNGTH	35937.91	
GVFVSNGT	42011.96	

C

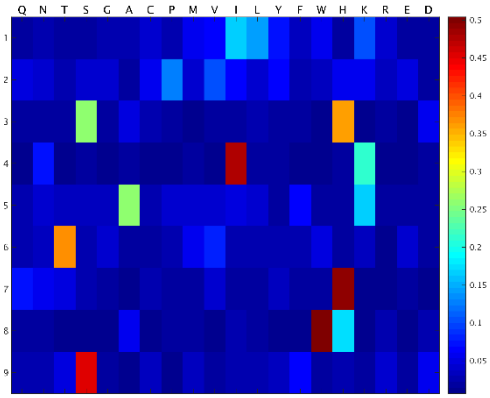

E

CPL score	Peptide	Affinity(nM)	Bindlevel
-15,2522	KPSIGEHWS	10598.08	
-17,0164	LISKQTHWY	163.63	<= WB
-17,1607	LNSIVTHLS	23849.06	
-17,5175	IPSINVHHY	33.76	<= SB
-17,5175	IPSINVHHY	27394.30	
-17,5175	IPSINVHHY	18294.40	
-17,8196	LEQIKTHWL	8368.07	
-17,8196	LEQIKTHWL	8964.47	
-17,8927	KPPIGEHWS	6409.98	
-17,9177	VPSIGEHWD	19051.95	

Supplementary figure 3 Peptide identification of 8UTT6 clone

A) Table showing T cell receptor sequencing result of UTT clones (N=23). B) Heatmap showing reactivity of a representative clone, 8UTT6 clone, against sub pools of SARS-CoV-2 spike peptide library loaded on K562s transduced with HLA-B*35:01. Reactivity was measured by IFN-γ ELISA. Peptides that induced highest IFN-γ production were depicted under the figure with amino acid overlap between the peptides in black. C) Table showing NetMHC 4.0-predicted binding to HLA-B*35:01 of peptides that were recognized in the spike peptide library. The 10 peptides with highest binding to HLA-B*35:01 are shown. D) Heatmap demonstrating peptide recognition signature of 8UTT6 clone using the CPL assay. 8UTT6 clone was co-cultured with peptide-loaded K562 cells

1013 transduced HLA-B*35:01. Secreted IFN-γ was measured by ELISA and corrected per row. E)
1014 Table showing the 10 peptides with highest CPL score and their binding affinity to HLA-B*35:01,
1015 as predicted by netMHC 4.0.

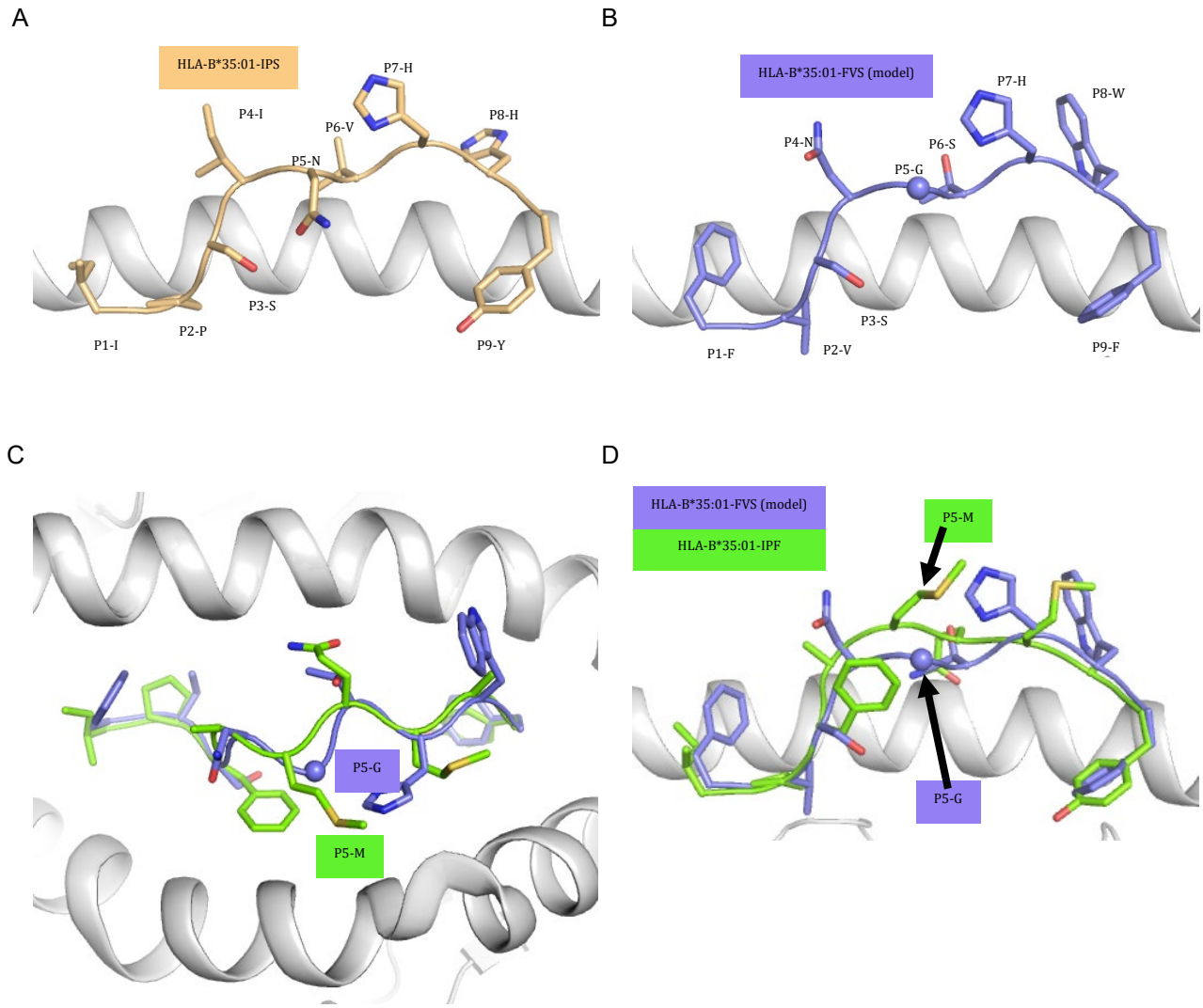

Supplementary Figure 4 Structural analysis of the HLA-B*35:01-FVS model

A-B) Structural overlay of HLA-B*35:01-IPF structure with the model of the HLA-B*35:01-FVS. C) Top view of the HLA-B*35:01-IPF (peptide in chartreuse) and HLA-B*35:01-FVS (peptide in blue) aligned on the HLA cleft (white cartoon). D) A side view of the same structural overlay as panel A, with the same colour scheme. The sphere represents the Cα atom of the FVS peptide P5-G residue.

A

	TRAV (IMGT)	TRAJ (IMGT)	CDR3 (aa)	CDR3α (nt)
UTT	TRAV21*02	TRAJ23*01	CAGNQGGKLIF	TGTGCTGGGAACCCAGGGAGGAAAGCTTATCTTC
UBV	TRAV21*01	TRAJ23*01	CAGNQGGKLIF	TGTGCTGGAAACCCAGGGAGGAAAGCTTATCTTC
JZX	TRAV21*02	TRAJ23*01	CAGNQGGKLIF	TGTGCTGGGAACCCAGGGAGGAAAGCTTATCTTC
SFW	TRAV21*02	TRAJ23*01	CAGNQGGKLIF	TGTGCTGGGAACCCAGGGAGGAAAGCTTATCTTC

B

	TRBV (IMGT)	TRBV (IMGT)	CDR3 (aa)	CDR3β (nt)
UTT	TRBV12-3*01	TRBJ2-1*01	CASSLALDEQFF	TGTGCCAGCAGTTTAGCGCTGGATGAGCAGTTCTTC
UBV	TRBV12-3*01	TRBJ2-1*01	CASSLALDEQFF	TGTGCCAGCAGTTTAGCGCTGGATGAGCAGTTCTTC
JZX	TRBV12-3*01/TRBV12-4*01	TRBJ2-1*01	CASSLALDEQFF	TGTGCCAGCAGTTTAGCGCTCGATGAGCAGTTCTTC
SFW	TRBV12-3*01/TRBV12-4*01	TRBJ2-1*01	CASSLALDEQFF	TGTGCCAGCAGTTTAGCGCTTGATGAGCAGTTCTTC

Supplementary figure 5 TCR sequencing of B*35/FVS-sorted samples

Nucleotide alignment of the CDR3 α and β sequence of PBMCs sorted on B*35/FVS-tetramer binding. Segment numbering is depicted according to the international immunogenetics information system (IMGT) nomenclature. A) Nucleotide alignment of the CDR3α sequences. B) Nucleotide alignment of the CDR3β sequences.

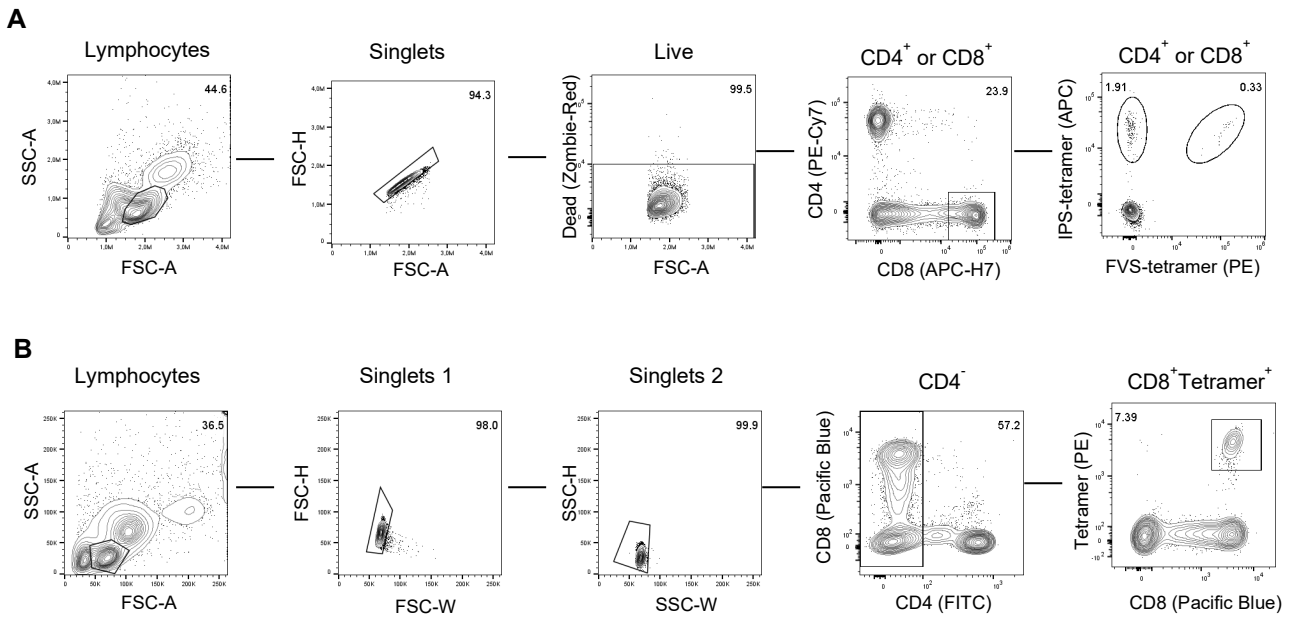

Supplementary figure 6 Flow cytometry and cell sorting gating example for tetramer staining assays

A) Representative example of flow cytometry gating strategy for tetramer positive $CD8^+$ T cells. All events were gated on lymphocytes, single cells, viable cells, CD8 positive and subsequently separated for binding to tetramer consisting of HLA-B*35:01 with IPS peptide or FVS peptide. B) Representative example of fluorescent-activated cell sorting for tetramer positive $CD8^+$ T cells. All events were gated on lymphocytes, single cells, $CD4^-$ and subsequently on $CD8^+$tetramer$^+$.

Supplementary Table 1 Cohort characteristics

Study code	CMV status	Storage date	HLA-A*		HLA-B*		HLA-C*		HLA-DRB1*		HLA-DRB3*		HLA-DRB4*	HLA-DRB5*		HLA-DQA1*		HLA-DQB1*		HLA-DPB1*	
UAB	Positive	18-02-15	02:01:01	68:01:02	15:01:01:01	35:08:01	03:04	04:01	04:01:01	10:01:01			01:03:01:01					03:02/03:11	05:01/05:51	02:01:02	04:02:01
UBD	Negative	14-06-11	01:01:01:01	02:01	15:01:01:01	51:01:01	03:04	14:02:01	08:03:02	15:01				01:01:01				03:01/03:21/03:22+	06:02/06:14/06:20	03:01:01	04:01:01
UBL	Positive	30-12-11	02:01:01		51:01:01	57:01:01	06:02:01	15:02:01	04:08:01	16:01:01			01:03:01:01	02:02				03:01:01	05:02:01	03:01/104:01	04:01
UBQ	Positive	28-01-11	01:01:01:01	11:01:01	08:01/08:50	15:01/15:142	03:03:01	07:01	03:01		01:01			01:01:01				02:01:01	06:02:01	02:01	04:01/81:01
UBT	Negative	10-04-14	02:01	25:01:00	15:01/15:50/15:225	18:01/18:36/18:43	04:01/04:94	12:03/12:24	03:01:01	04:04:01	01:01:02		01:03:01:01					02:01:01	03:02:01	04:01:01	
UBV	Positive	24-04-13	01:01:01:01	03:01:01	08:01:01	35:01/35:42	04:01/04:82	07:01/07:06/07:18	01:01:01	03:01:01	01:01:02							02:01:01	05:01:01	04:01:01	
UBW	Positive	19-05-15	02:01	23:01/23:17	15:01:01:01	44:03:01	03:03:01	04:01/04:82	07:01:01	15:01:01			01:01:01:01	01:01:01				02:02:01	06:02:01	04:01:01	
UBZ	Negative	8-02-13	02:01:01		15:01:01:01	51:01:01	03:03:01	15:02:01	04:08:01	13:01:01	01:01:02		01:03:01:01			01:03:01	03:03:01	03:01	06:03	02:01:02	04:02:01
UCU	Negative	23-04-15	01:01:01:01	29:02:01	08:01:01	44:03:01	07:01/07:343	16:01:01	03:01:01	07:01:01	01:01:02		01:01:01:01					02:01:01	02:02:01	01:01:01	11:01:01
UDB	Negative	19-10-16	03:01:01	31:01:02	07:02:01	27:05:02	02:02/02:13/02:43	07:02/07:15/07:241	04:01:01	15:01:01			01:03:01:01	01:01:01				03:02:01	06:02:01	04:01:01	
UDP	Positive	20-08-18	02:01:01	68:01/68:152	07:02:01	38:01:01	07:02	12:03:01	04:05:01	15:01:01			01:03:01:01	01:01:01				03:02:01	06:02:01	03:01/104:01/124:01	04:01/350:01
UDS	Positive	30-06-16	01:01:01:01	02:01:01	08:01:01	18:01:01	05:01/05:98	07:01/07:343/07:73	03:01:01		01:01/01:15	02:02/02:21						02:01:01		03:01/104:01/124:01	04:01/350:01
UDV	Positive	4-08-15	01:01	11:01	08:01	55:01:00	03:03	07:01	03:01/03:13	14:54	01:01							02:01	05:03	04:01	
UEN	Positive	27-08-18	01:01/01:17	03:01/03:08	07:02/07:26/07:61	57:01/57:19	06:02	07:02	03:01		01:01			01:01				02:01	06:02:01	01:17,0	
UES	Positive	29-08-13	02:01:01	68:01:01	07:02:01	44:03:01	07:02:01	16:01:01	07:01:01	15:01:01			01:01:01:01	01:01:01				02:02	06:02:01	04:01:01	13:01/107:01
UFL	Positive	15-03-17	11:01:01	66:01:01	55:01:01	58:02:01	03:03/03:18	06:02/06:70	04:07/04:92	15:03:01			01:03:01:01	01:01:01				03:01:01	06:02:01	02:01/414:01/461:01	03:01/104:01/124:01
UFU	Negative	2-04-17	03:01:01		07:02:01	51:01:01	07:02:10	14:02	04:01:01	15:01:01			01:03:01:01	01:01:01				03:02/03:08	06:02/06:48	04:01:01	
UGI	Negative	20-11-17	02:01/02:665		15:01/15:225	27:05/27:37	01:02	03:04	01:03	04:01:01								03:01/03:138	03:02/03:74		
UGM	Negative	10-04-19	02:01:01	31:01:02:01	07:02:01:01	44:03:01	07:02:01	16:01:01:01	01:01:01	07:01/07:79			01:01:01:01			01:01:01	02:01:01	02:02:01	05:01:01	01:01:01	
UGT	Positive	27-06-17	01:01:01:01	02:01:01	51:01:01	57:01:01	06:02:01	14:02:01	03:01:01	11:01:01	01:01/01:15	02:02/02:21						02:01:01	03:01:01	04:01:01	
UGV	Negative	9-02-16	01:01:01:01	32:01:01	44:02:00	57:01:01	05:01:01	06:02:01	07:01:01	12:01/12:10	02:02:01		01:03:01:02N					03:01/03:12	03:03/03:69	01:01/417:01	04:02:01
UGZ	Negative	3-01-19	02:01	03:01:01	07:02:01	35:01:01	04:01:01	07:02:01	01:01:01	15:01:01				01:01:01				05:01	06:02:01	02:01	03:01:01
UHC	Negative	11-06-18	02:01:01	24:02/24:353	15:01:01	40:01:00	03:03/03:341	03:04:01	07:01:01	13:01:01	02:02:01		01:03:01:01					02:02:01	06:03:01	10:01:01	124:01
UHJ	Positive	20-11-17	03:01:01	03:02:01	18:01/18:80	44:02/44:221	12:03:01	16:04:01	04:02:01	11:04:01	02:02:01		01:03:01:01					03:01:01	03:02:01	04:01/126:01	04:02/105:01
UHL	Negative	21-08-15	02:01:01	30:01:01	13:02	18:01	05:01:01	06:02:01	03:01:01	13:01:01	01:01/01:15			02:02/02:21				02:01:01	06:03:01	04:01:01	17:01
UHO	Negative	8-03-19	26:01:01		07:02:01	38:01:01	07:02:01	12:03:01	15:01:01					01:01:01				06:02:01	06:03:01	04:01:01	
UHS	Negative	6-10-14	03:01:01	24:02:00	18:01:01	44:02:00	05:01	07:01	11:04:01	13:01:01	01:01/01:15	02:02/02:21						03:01:01	06:03:01	04:01/105:01	04:02/126:01
UHZ	Negative	8-10-14	02:01/02:323	66:01/66:06	14:02:01	58:01:01	03:02:02	08:02:01	01:02:01	13:02:01	03:01:01							05:01:01	06:09:01	02:01:02	04:01:01
UJC	Negative	15-04-19	02:01:01:05	11:01:01:01	07:02:01:01	27:05:02	01:02:01	07:02:01	01:01:01							01:01:01		05:01:01		02:01:02	04:01:01
UJO	Positive	25-01-18	11:01	24:02/24:353	35:03:01	55:01:01	03:03	04:01	01:01:01	14:54:01	02:02:01							05:03:01	05:04	03:01/104:01/124:01	04:01/350:01
UJS	Negative	21-09-11	03:01/03:37/03:09		07:02:01		07:02		03:01	04:04:01	01:01:00		01:03:01:01					02:01:01	03:02:01		
UKI	Negative	6-07-15	02:01:01	68:01:01	08:01	15:01:01:01	03:03/03:18	07:01/07:343/07:263	03:01:01	13:01:01	01:01/01:15	02:02/02:21						02:01:01	06:03:01	04:01:01	13:01/107:01
UKU	Positive	14-11-18	02:01:01		44:02:01		05:01:01		01:01:01	04:01:01			01:03:01:01					03:01:01	05:01:01	02:01:02	04:02:01
UKY	Negative	31-03-15	24:02:00	29:02:01	15:01:01:01	44:03:01	03:03:01	16:01:01	13:01:01	15:01:01	02:02:01			01:01:01				06:02:01	06:03:01	02:01:02	04:01:01
UKZ	Negative	25-09-12	02:01	03:01	15:01	57:01:00	03:04	06:02	04:01				01:03					03:02		04:01	
ULL	Negative	27-10-14	03:01:01	26:01:01	08:01:01	55:01:01	03:03:01	07:01	03:01:01	14:54:01	01:01/01:15	02:02/02:21						02:01:01	05:03:01	01:01:01	04:01:01
UML	Negative	1-11-06	03:01	24:02/24:09N/24:17+	27:02:00	40:01:00	02:02	03:04	08:01		01/02/03N	02:02						03:01:01	04:02	01:04,0	
UMV	Negative	19-11-13	01:01:01:01	03:01:01	07:02/07:61	44:02:01	07:02:01	07:04:01	04:01:01	13:02:01	03:01:01		01:03:01:01					03:02:01	06:04:01	04:01:01	
UNF	Positive	22-09-16	24:02:00	68:01:02	35:02:01	44:02:00	04:01/04:82	07:04:01	11:01:01	11:04:01	02:02:01							03:01:01		04:01:01	
UNK	Positive	21-01-15	01:01:01:01	02:01:01	08:01	15:01:01	03:03/03:18	07:01/07:343/07:263	13:02:01	16:01:01	03:01:01			02:02				05:02/05:01	06:04/06:25	03:01/104:01	04:01:01
UPF	Negative	27-12-18	03:01:01:01	31:01:02:01	27:02:01:01	27:05:02	01:02:01	02:02:02:03	01:01:01	16:01:01				02:02:01		01:01:01	01:02:02	05:01:01	05:02:01:01	02:01/416:01	04:02/105:01
UPJ	Positive	17-03-14	03:01:01		07:02:01	40:02:01	02:02:02	07:02:01	03:01:01	15:01:01	01:01:02			01:01:01				02:01:01	06:02:01	03:01/104:01	04:01:01
UPN	Negative	1-08-18	01:01/01:234	31:01/31:119	08:01/08:173	15:01:01	03:04/03:294	07:01/07:153	03:01:01	04:01:01	01:01:02		01:03:01:01					02:01/02:54	03:02/03:221	01:01/417:01	04:01:01
UQS	Negative	21-07-16	01:01/01:43	11:01/11:199	08:01	40:02:01	02:02:02	07:01:01	03:01:01	11:01:01	01:01/01:15	02:02/02:21						02:01:01	03:01:01	01:01/417:01	04:01/278:01
UQT	Positive	21-06-17	68:01:02	68:02:01	41:02:01	44:02:01	07:04:01	17:01:01	07:01:01	13:02:01	03:01:01		01:03/01:134					02:02:01:01	06:04:01	04:01/350:01	39:01/584:01
URG	Negative	16-04-15	02:01	24:02:00	07:02:01	35:02:01	04:01/04:82	07:02	07:01:01	15:01:01			01:01:01:01	01:01:01				02:02:01	06:02:01	02:01:02	04:01:01
URJ	Negative	25-03-15	03:01/03:127	11:01/11:20	08:01	35:01/35:42	04:01	07:01	01:01:01	03:01:01	01:01:02							02:01:01	05:01:01	04:01:01	
URK	Positive	24-10-13	01:01:01:01	02:01:01	08:01:01	35:03:01	04:01/04:82	07:01	03:01:01	14:54	01:01/01:15	02:02/02:21						02:01:01	05:03:01	01:01:01	04:01:01
URU	Negative	2-06-14	02:01	24:02:00	15:01	51:01:00	03:03:01	14:02:01	08:01	13:01:01	02:02:01							04:02:01	06:03:01	03:01/104:01	03:01/104:01
URV	Negative	14-09-11	03:01		07:02/07:61	35:01/35:42	04:01	07:02	01:01:01	14:54	02:02							05:01:01	05:03:01	02:01:02	04:01:01
USB	Negative	15-12-15	01:01:01:01	03:01:01	07:02:01	35:02:01	04:01/04:82	07:02	11:04:01	15:01:01	02:02:01			01:01:01				06:02:01	06:03:01	02:01:02	04:01:01
USD	Negative	30-05-18	01:01:01		37:01:01	57:01:01	06:02:01		07:01:01	15:01:01			01:03:01:02N	01:01:01				03:03:02	06:02:01	03:01/104:01/124:01	04:01/350:01
USH	Negative	12-11-14	03:01:01	25:01:01	18:01:01	27:02:01	02:02:02	12:03:01	15:01:01	16:01:01				01:01/01:07	02:02/02:04			05:02:01	06:03:01	02:01:02	04:02:01
USI	Negative	20-04-15	01:01/01:89	24:02/24:120	07:02:01	41:01:00	07:02/07:50	17:01/17:03/17:02	07:01:01	15:01:01			01:01:01:01	01:01:01				03:03:02	06:02:01	04:01:01	17:01
USY	Negative	15-11-12	02:01:01		18:01/18:17N/18:43	44:02/44:19N/44:55	05:01	07:01	08:01	09:01:02			01:03:01:01					03:03:02	04:02:01	02:01:02	03:01:01
UTT	Positive	3-08-15	02:01:00	3:01:00	14:02:01	51:01:01	08:02:01	15:02:01	04:05:01	07:01:01			01:01:01:01, 01:03:01:01					02:02/02:31	03:01/03:73	03:01/104:01	04:01
UUC	Positive	5-01-16	01:01/01:89	24:02/24:120	07:02/07:114	08:01/08:151	07:01:01	07:02:01	03:01:01	11:01:01	01:01/01:15	02:02/02:21						02:01:01	03:01:01	01:01/417:01	02:01:02
UUG	Negative	27-10-16	02:01:01	32:01:01	15:01/15:247	44:02/44:27	03:03	05:01	04:01:01	15:02:01			01:03:01:01	01:02				03:02:01	06:01	02:01:02	04:01:01
UVA	Positive	23-03-17	01:01:01:01		37:01:01	57:01:01	06:02:01		07:01:01	10:01:01			01:03:01:02N					03:03:02	05:01:01	04:02	
UVF	Positive	13-02-12	02:01	68:01:02	18:01/18:17N/18:20	44:02/44:19N/44:51	05:01/05:23	07:04/07:12	11:01:01	15:01	02:02			01:01:01				03:01/03:21/03:22	06:02/06:19/06:20	02:01:02	04:01:01
UVO	Positive	2-04-19	01:01:01	11:01	08:01/08:182	35:01/35:42/35:347	04:01:01	07:01:01	03:01:01	11:01:01	01:01:02	02:02:01						02:01/02:82	03:01/03:264	01:01/162:01/417:01	04:01/350:01
UWI	Negative	12-01-15	02:01	24:02:00	07:02:01	40:02:01	02:02:02	07:02:01	03:01:01	07:01:01	01:01:02		01:03:01:01					02:01:01	02:02:01	01:01:01	04:01:01
UWT	Positive	5-04-11	03:01	32:01:01	39:06:02	40:01:02	03:04	07:02	01:01:01	04:04:01			01:03:01:01					03:02:01	05:01:01	02:01:02	06:01
UWU	Negative	5-06-14	03:01:01	32:01:01	35:01/35:42	51:01:01	04:01/04:33	14:02/14:13	01:01:01	11:01:01	02:02:01							03:01:01	05:01:01	04:01:01	13:01/107:01
UXY	Positive	10-07-18	01:01:01	02:01/02:665	13:02	44:03:00	06:02:01	16:02:01	04:02:01	07:01:01			01:03:01:01					02:02/02:54	03:02/03:221	02:01	04:01:01
UYS	Negative	28-02-19	01:01:01:01	03:01:01:01	08:01:01:01	27:05:02	02:02:02:01	07:01:01	03:01:01	04:01:01	01:01:02		01:03:01:01			03:03:01:01	05:01:01:02	02:01:01	03:01:01	04:01/126:01	04:02/105:01/665:01
UZZ	Positive	1-08-13	01:01:01:01	24:02:01	07:02	08:01	07:01:01	07:02:01	01:01:01	04:04:01			01:03:01:01					03:02:01	05:01:01	04:01/105:01	04:02/126:01

1039 **Supplementary Table 2** List of peptides

1040

Peptide pools					
Name in study	**Antigen**	**Pathogen**	**Supplier**	**Catalogous #**	**Characteristics**
S	Spike	SARS-CoV-2	Miltenyi	130-126-701	15-mer, 11aa overlap
S1	Spike	SARS-CoV-2	Miltenyi	130-127-041	15-mer, 11aa overlap
S+	Spike	SARS-CoV-2	Miltenyi	130-127-312	15-mer, 11aa overlap
M	Membrane	SARS-CoV-2	Miltenyi	130-126-703	15-mer, 11aa overlap
N	Nucleocapsid	SARS-CoV-2	Miltenyi	130-126-699	15-mer, 11aa overlap
pp65	pp65	CMV	JPT	Custom-made	15-mer, 11aa overlap
pp65 library	pp65	CMV	JPT	Custom-made	15-mer, 11aa overlap
Spike library	Spike	SARS-CoV-2	SB Peptides	SB043	15-mer, 11aa overlap

Single peptides					
Sequence	**Antigen**	**Pathogen**	**Supplier**	**Catalogous #**	**Characteristics**
VFTWPPWQAGILARN	pp65	CMV	LUMC	Custom-made	15-mer
PPWQAGILARNLVPM	pp65	CMV	LUMC	Custom-made	15-mer
AGILARNLVPMVATV	pp65	CMV	LUMC	Custom-made	15-mer
ARNLVPMVATVQGQN	pp65	CMV	LUMC	Custom-made	15-mer
VPMVATVQGQNLKYQ	pp65	CMV	LUMC	Custom-made	15-mer
AQGDDDVWTSGSDSD	pp65	CMV	LUMC	Custom-made	15-mer
SSATACTSGVMTRGR	pp65	CMV	LUMC	Custom-made	15-mer
PKRRRHRQDALPGPC	pp65	CMV	LUMC	Custom-made	15-mer
FVSNGTHWF	Spike	SARS-CoV-2	LUMC	Custom-made	9-mer
IPSINVHHY	pp65	CMV	LUMC	Custom-made	9-mer

1041 **Supplementary Table 3** List of antibodies and reagents used for flow cytometry

Antibodies						
Antigen	**Target species**	**Format**	**Clone**	**Supplier**	**Catalogous #**	**RRID**
CCR7	Human	BV711	3d12	BD Biosciences	563712	AB_2738386
CD137	Human	APC	4B4-1	BD Biosciences	550890	AB_398477
CD14	Human	FITC	M5E2	BD Biosciences	555397	AB_395798
CD154	Human	Pacific Blue	24-31	Biolegend	310820	AB_830699
CD19	Human	FITC	HIB 19	BD Biosciences	555412	AB_395812
CD4	Human	PE-Cy7	SFCI12TD4	Beckham Coulter	737660	AB_2922769
CD4	Human	FITC	RPA-T4	BD Biosciences	555346	AB_395751
CD4	Human	BV510	SK3	BD Biosciences	562970	AB_2744424
CD45RA	Human	PE-Texas-Red	MEM-56	Invitrogen	MHCD45RA17	AB_10372222
CD8	Human	APC-H7	SK1	BD Biosciences	560179	AB_1645481
CD8	Human	PE-Cy7	RPA-T8	BD Biosciences	557746	AB_396852
CD8	Human	Pacific Blue	RPA-T8	BD Biosciences	558207	AB_397058
IFNγ	Human	Alexa-Fluor 700	4S.B3	Sony	3112600	AB_2922770
IFNγ	Human	BV711	B27	BD Biosciences	564039	AB_2738557
HLA-DR	Human	Alexa-Fluor 700	G46-6	BD Biosciences	560743	AB_1727526
CD38	Human	BV605	HIT2	BD Biosciences	740401	AB_2740131
CD19	Mouse	PE	1D3	BD Biosciences	557399	AB_396682

Other reagents		
Product	**Supplier**	**Catalogous #**
Zombie-Red	Biolegend	423109
Zombie-Aqua	Biolegend	423101
Brilliant Violet Stain Buffer Plus	BD Biosciences	566385
Beta Mark TCR Vbeta Repertoire Kit	Beckham Coulter	IM3497

1042

1043 **Supplementary Table 4** List of primer sequences used for TCR sequencing

1044

1045

Description	Name	Nucleotide sequence 5'►3'
cDNA primer	anchored oligo-dT primer	AAGCAGTGGTATCAACGCAGAGTACT30VN, where "N" is any base and "V" is either "A", "C" or "G"
cDNA primer SmartSeq2modified template switching oligo	SS2m_TSO	AAGCAGTGGTATCAACGCAGAGTACAT(G)(G){G}
Pre amplification PCR primer	IS PCR	AAGCAGTGGTATCAACGCAGAGT
PCR primer SmartSeq2modified forward	SS2m_For	GAGTTCAGACGTGTGCTCTTCCGATCTAAGCAGTGGTATCAACGCAGAGTACAT
PCR primer TRAC reverse	TRAC_rev	CCTACACGACGCTCTTCCGATCTACGGCAGGGTCAGGGTTCTGGATAT
PCR primer TRBC1 reverse	TRBC1_rev	CCTACACGACGCTCTTCCGATCTGTGGGAACACCTTGTTCAGGTCCT*C
PCR primer TRBC1 reverse	TRBC2_rev	CCTACACGACGCTCTTCCGATCTGTGGGAACACGTTTTTCAGGTCCT*C
Barcode primer SS2m region, forward, backbone	BC_R7xx_For	CAAGCAGAAGACGGCATACGAGAT$_{nnnnnn}$GTGACTGGAGTTCAGACGTGTGCTCTTCCGAT*C
Barcode primer region, reverse, backbone	BC_R7xx_Rev	AATGATACGGCGACCACCGAGATCTACAC$_{nnnnnn}$ACACTCTTTCCCTACACGACGCTCTTCCGATC*T

Abbreviations: TRA: T-cell Receptor Alpha, TRB: T-cell Receptor Beta, SS2m: SmartSeq2Modified, TSO: Template Switching Oligo, TRAC: T-cell Receptor Alpha Constant, TRBC: T-cell Receptor Beta Constant, For: Forward, Rev: Reverse, AC: Alpha chain, BC: Beta chain, nnnnnn: Identifier sequence

()=RNA, {}=LNA: Locked Nucleic Acid, *:phosphonothioate-binding